JACS
JOURNAL OF THE AMERICAN CHEMICAL SOCIETY
Article
Cite This: J. Am. Chem. Soc. XXXX, XXX, XXX−XXX
pubs.acs.org/JACS

Substrate-Based Allosteric Regulation of a Homodimeric Enzyme

Pedram Mehrabi,[†,‡,§,▽] Christopher Di Pietrantonio,[∥,▽] Tae Hun Kim,[∥,⊥,▽] Adnan Sljoka,[∥,#,⊗] Keith Taverner,[∥] Christopher Ing,[⊥,+] Natasha Kruglyak,[§,+] Régis Pomès,[⊥,+] Emil F. Pai,[*,†,§,+,¶] and R. Scott Prosser[*,†,∥,+,¶]

[†]Department of Medical Biophysics, University of Toronto, Toronto, Ontario M5G 1L7, Canada
[‡]Department for Atomically Resolved Dynamics, Max-Planck-Institute for Structure and Dynamics of Matter, Luruper Chaussee 149, 22761 Hamburg, Germany
[§]Campbell Family Institute for Cancer Research, Princess Margaret Cancer Centre, Toronto, Ontario M5G 1L7, Canada
[∥]Department of Chemistry, University of Toronto, UTM, 3359 Mississauga Road North, Mississauga, Ontario L5L 1C6, Canada
[⊥]Program in Molecular Medicine, Research Institute, The Hospital for Sick Children, Toronto, Ontario M5G 0A4, Canada
[#]CREST, Japan Science and Technology Agency (JST), Department of Informatics, School of Science and Technology, Kwansei Gakuin University, Sanda 669-1337, Japan
[+]Department of Biochemistry, University of Toronto, 1 King's College Circle, Toronto, Ontario M5S 1A8, Canada
[⊗]Center for Advanced Intelligence Project, RIKEN, 1-4-1 Nihombashi, Chuo-ku, Tokyo 103-0027, Japan

Supporting Information

ABSTRACT: Many enzymes operate through half-of-the sites reactivity wherein a single protomer is catalytically engaged at one time. In the case of the homodimeric enzyme, fluoroacetate dehalogenase, substrate binding triggers closing of a regulatory cap domain in the empty protomer, preventing substrate access to the remaining active site. However, the empty protomer serves a critical role by acquiring more disorder upon substrate binding, thereby entropically favoring the forward reaction. Empty protomer dynamics are also allosterically coupled to the bound protomer, driving conformational exchange at the active site and progress along the reaction coordinate. Here, we show that at high concentrations, a second substrate binds along the substrate-access channel of the occupied protomer, thereby dampening interprotomer dynamics and inhibiting catalysis. While a mutation (K152I) abrogates second site binding and removes inhibitory effects, it also precipitously lowers the maximum catalytic rate, implying a role for the allosteric pocket at low substrate concentrations, where only a single substrate engages the enzyme at one time. We show that this outer pocket first desolvates the substrate, whereupon it is deposited in the active site. Substrate binding to the active site then triggers the empty outer pocket to serve as an interprotomer allosteric conduit, enabling enhanced dynamics and sampling of activation states needed for catalysis. These allosteric networks and the ensuing changes resulting from second substrate binding are delineated using rigidity-based allosteric transmission theory and validated by nuclear magnetic resonance and functional studies. The results illustrate the role of dynamics along allosteric networks in facilitating function.

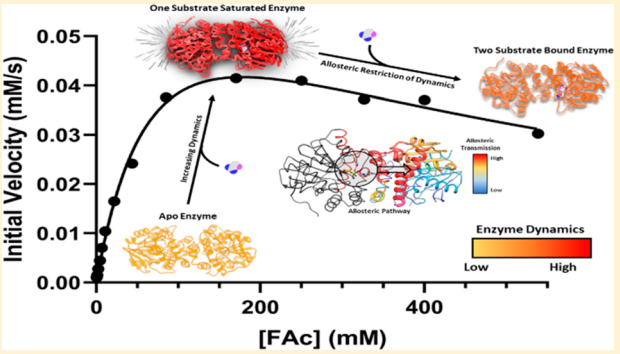

INTRODUCTION

Many enzymes have evolved to attain remarkable catalytic efficiency and specificity.[1] While their structure provides the appropriate environment for substrate recognition and specificity, dynamics also play a key role in the process. For example, enzyme flexibility facilitates sampling of conformers which serve to capture and position substrate(s) in the active site, undergo the requisite chemical steps, and release product(s).[2−6] Enzyme activities are tightly regulated in many cellular processes, often through binding of inhibitors at either allosteric or catalytic sites. In upward of 20% of enzymes, the substrate itself may serve as an inhibitor, begging the question of how an enzyme which has evolved to be maximally efficient for a given substrate can at the same time be inhibited when substrate is in excess.[7] There are many situations in living systems where substrate inhibition is a functional necessity. A well-known example involves acetylcholinesterase, which is inhibited in the early phase of signaling where high transient concentrations of acetylcholine are meant to engage receptors in the postsynaptic membrane. As free acetylcholine concentrations drop, acetylcholinesterase must

Received: April 6, 2019
Published: June 12, 2019

Downloaded via GUILFORD COLG on July 22, 2019 at 08:20:48 (UTC).
See https://pubs.acs.org/sharingguidelines for options on how to legitimately share published articles.

© XXXX American Chemical Society

DOI: 10.1021/jacs.9b03703
J. Am. Chem. Soc. XXXX, XXX, XXX−XXX

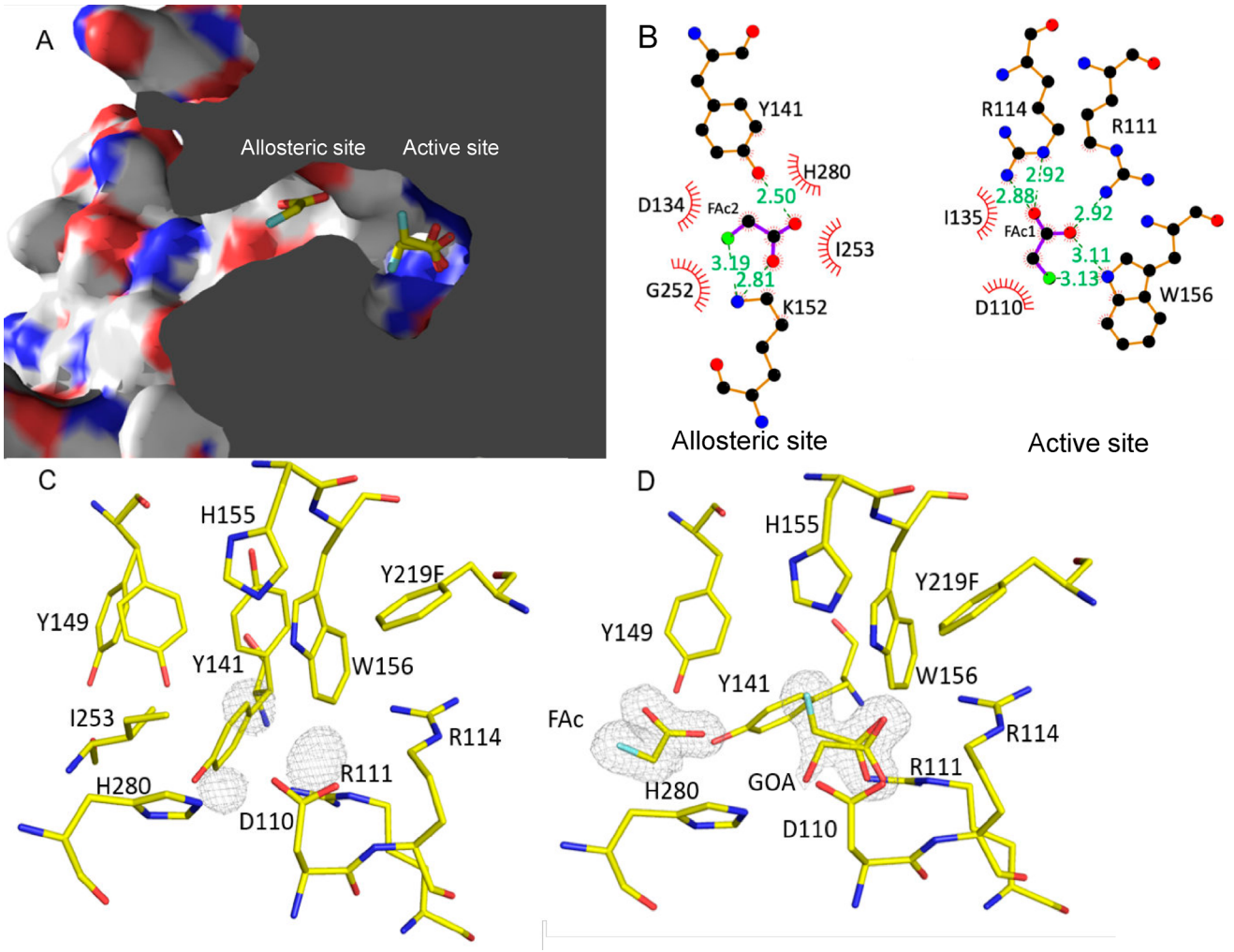

Figure 1. Multiple binding sites of substrate molecules in the slow Y219F mutant.(A) A cross-section through one protomer of FAcD displaying the substrate access channel from the protein surface to the active site. Under high concentrations of substrate, a second substrate binding site is revealed in the access channel of the bound protomer, where the side chain of I253 from the cap domain, is displaced by binding of FAc. (B) LigPlots[59] of the two substrate molecules showing the contacts between ligands and protein for each of the binding sites. Two hydrogen bonds link the carboxylic oxygens of FAc to the side chains of Y141 and K152 in the second pocket. In contrast, there are five binding interactions between FAc and other residues in the active site. (C and D) $2F_o$-F_c electron density map contoured at 1σ around the end of the substrate access channel of FAcD. (C) In the empty protomer, only water molecules and a chloride ion can be seen while the other protomer (D) holds the two substrate molecules at adjacent locations.

efficiently catalyze the compound's rapid degradation to terminate nerve impulse transmission.[7,8] In the current study, we present results regarding the phenomenon of substrate inhibition and the allosteric mechanisms at play for a homodimeric enzyme, fluoroacetate dehalogenase (FAcD) from *Rhodopseudomonas palustris*.

As the majority of enzymes are oligomeric, one might anticipate that the most common form of substrate inhibition might involve binding of additional substrate(s) to unoccupied protomers resulting in inactivation or attenuation of catalysis through allosteric inhibition of the overall oligomer.[7,9−11] Alternatively, within a given subunit, we can envisage a second substrate binding site along the access path to the active site. In this case, binding by a second substrate would be expected to slow access of substrate to (and egress of product from) the active site.[8] A third possibility would be that the substrate binds to an entirely different site, not associated with either the active sites or the access path, resulting in allosteric inhibition. Recent spectroscopic and crystallographic studies of FAcD reveal that it undergoes catalysis through half-of-the-sites reactivity,[12−16] where empty protomer dynamics and interprotomer allostery initiated by substrate binding greatly influence catalysis.[17] Upon binding a single substrate, access of substrate to the active site in the empty protomer is strictly prevented by a dynamic regulatory cap domain, discussed below. Second site substrate binding nevertheless occurs, albeit in an allosteric pocket along the substrate access channel associated with the occupied protomer. However, since the catalytic rate is much slower than the off-rate for the second substrate, product egress is not significantly attenuated. Rather, the allosteric pocket is shown here to be a hub for interprotomer allosteric transmission. Thus, simultaneous binding by substrates to both the active site and the allosteric pocket restrict both allosteric transmission and dynamics of the enzyme resulting in a loss in catalytic efficiency. In contrast, at low substrate concentrations, this same allosteric pocket enhances catalytic efficiency. This is achieved through a process in which the substrate is first desolvated and then deposited into the active site, triggering a

DOI: 10.1021/jacs.9b03703
J. Am. Chem. Soc. XXXX, XXX, XXX−XXX

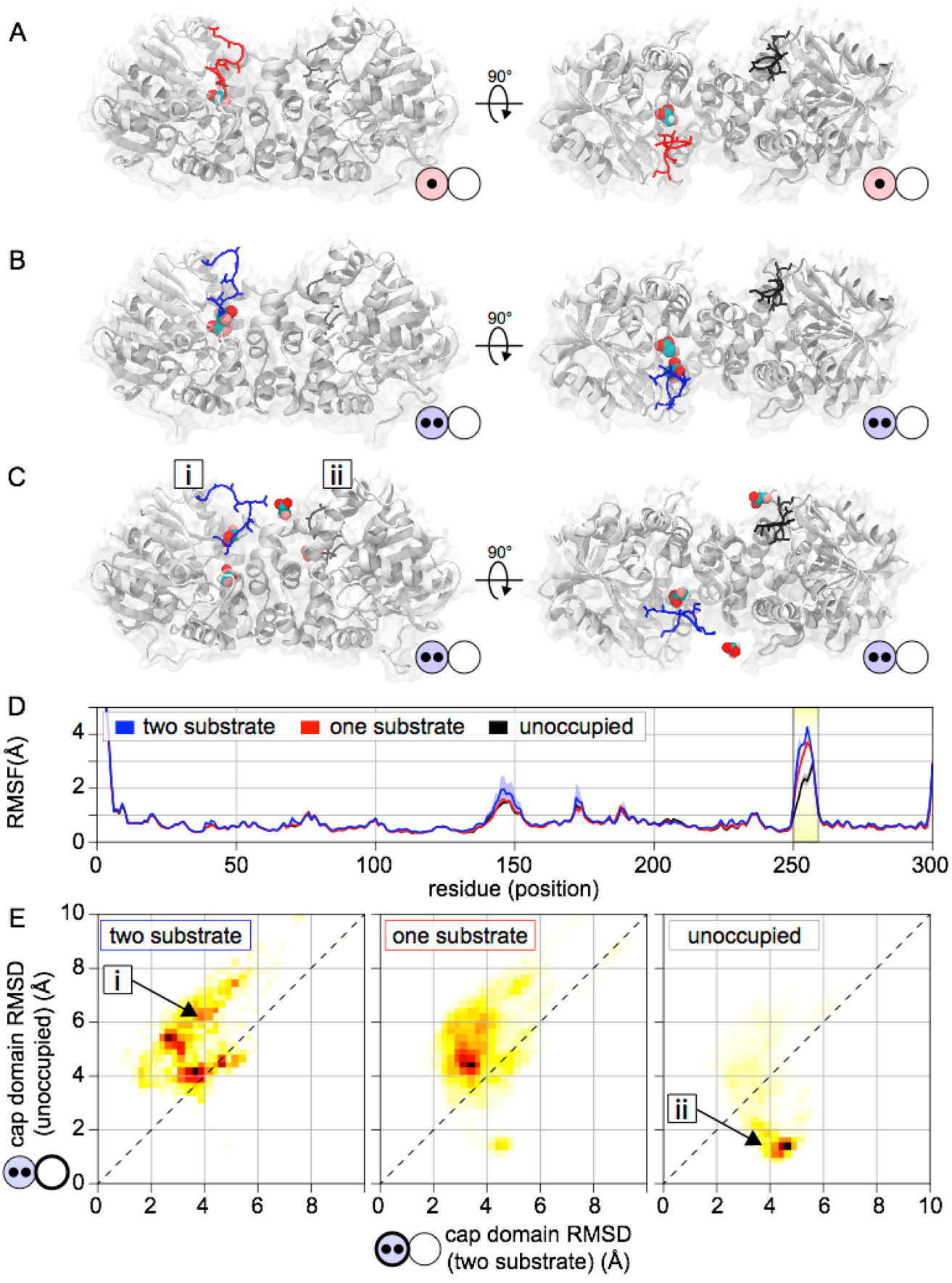

Figure 2. The regulatory cap domain exhibits fluctuations correlated with binding of substrates in the active site. (A) X-ray crystal structure of FAcD, bound to one FAc substrate, contrasting the distinct orientations of the cap domain in the substrate-bound and free protomers. (B) X-ray

DOI: 10.1021/jacs.9b03703
J. Am. Chem. Soc. XXXX, XXX, XXX−XXX

Figure 2. continued

crystal structure of FAcD, in which two substrates are observed to bind to one protomer. In this case, the regulatory cap of the empty protomer can be seen to adopt a more pronounced "closed" state, implying an allosteric response, mediated by second substrate binding. (C) MD trajectory snapshot of FAcD in which two substrates remain bound to one protomer and alternate conformations of the regulatory cap domains can be observed. (D) Root-mean-square fluctuations for different substrate occupancy states of the monomer. This analysis reveals that the amino acids forming the cap domain undergo significant fluctuations in an occupancy-state-dependent manner (0 < 1 < 2 FAc). (E) Root mean square deviation of the cap domain Cα atoms with respect to the crystallographic structure of the substrate-bound and empty protomer depicted in panel B. Reduction of cap domain excursions from the empty protomer reference state occurs in an occupancy dependent manner. The cap domain of the substrate-bound protomers can adopt diverse conformational states with high deviation from the reference structure, whereas the substrate-free protomer adopts a single conformation close to the crystallographic structure.

dynamic response conducted through this allosteric hub, enabling sampling of activation states needed for catalysis. The mechanisms associated with this exquisite regulation and the role of the second pocket in interprotomer allostery are discussed below.

FAcD catalyzes the hydrolysis of carbon halogen bonds, specifically the C−F bond, generating glycolate, a halide ion, and a proton as products. In previous studies, we determined the crystal structures of key catalytic intermediates, some of them stabilized by mutations of residues involved in catalysis.[17,18] In particular, the Michaelis−Menten complex structure determined by cocrystallizing the D110N mutant of FAcD with substrate showed substrate bound at only one of the dimer's active sites.[17] To enable time-dependent crystallographic experiments, we have made use of a mutant (Y219F) whose unusually low catalytic rate (k_{cat} = 0.035 min^{-1}) allows us to extend substrate soaking times in protein crystals from minutes to hours. This makes it possible to capture successive functional poses such as the Michaelis−Menten complex and a product-bound state as a crude function of time, using freeze trapping X-ray crystallography. While the catalytic mechanism is similar in both wild type (WT) FAcD and Y219F, the absence of the hydroxyl group in the mutant likely compromises electrostatic stabilization of the leaving halide, thereby slowing catalysis. While the D110N mutant allows us to trap the Michaelis−Menten complex effectively, the H280N mutant largely prevents a subsequent hydrolysis step, thereby trapping the covalent intermediate. At high substrate concentrations, it is possible with H280N to first saturate the active site with a covalent intermediate and subsequently observe binding of substrate exclusively to the allosteric pocket. Thus, by performing substrate binding studies with D110N and H280N (upon saturation of the active site with a covalent intermediate), we are able to identify dissociation constants and interaction kinetics to both the active site and the allosteric pocket.

X-ray crystallography showed the substrate in the allosteric pocket is directly coordinated by Lys 152 and Tyr 141, within the substrate binding channel (Figure 1A). The mutation, K152I, abrogates second site binding and substrate inhibition, as will be shown. Surprisingly, K152I also results in a precipitous drop in the catalytic rate even at low substrate concentrations. This suggests that the allosteric binding pocket is not simply the origin of substrate inhibition but may also play a role in supporting catalysis. In this paper, we seek to understand how the allosteric pocket serves to enhance catalysis at low substrate concentrations, why the homodimer acts exclusively through half-of-the-sites reactivity, and more broadly, how allosteric networks operate between protomers in the dimer. Given that this thermophilic enzyme possesses 9 distinct tryptophan residues within the hydrophobic interior of each protomer, ^{19}F NMR of fluorotryptophan-enriched FAcD provides a convenient readout of local mobility, additional excited states, and allosteric interprotomer dynamics. Together, crystallography, ^{19}F NMR, and (^{15}N,^{1}H) NMR experiments of WT FAcD, D110N (Michaelis−Menten intermediate), Y219F (slow mutant), H280N (covalent intermediate), and K152I (deletion of allosteric pocket) provide new insights into allosteric processes, mechanisms of substrate inhibition, and the role of the allosteric pocket in enhancing catalysis under nonsaturating substrate concentrations.

RESULTS

Crystallography Reveals Two Substrate Molecules in One Protomer under Excess Substrate. To monitor progression of binding events associated with substrate inhibition, we made use of freeze-trapping X-ray crystallography.[19] Using a catalytically slow mutant (Y219F), it became possible to capture substrate-bound states and the subsequent generation of product in the active site, after soaking the crystals in 200 mM substrate from 30 min up to 24 h, followed by flash-freezing. Beginning with substrate-free Y219F, a progression of states can be captured from the active site binding two waters and a halide ion to binding of FAc substrate and formation of a putative glycolate product complex (Figure S1). Interestingly, using higher substrate concentrations in the soaking buffer we observed an intermediate complex containing two substrate molecules in one protomer, while the other protomer remained empty, consistent with half-of-the-sites reactivity.[17] As shown in Figure 1A,D, one of the two substrates adopts a position and orientation that closely overlaps with that in the Michaelis−Menten complex, while the second substrate molecule is 6 Å away, adjacent to the dimer interface and the cap domain, along the channel connecting the active site with the protein exterior. In contrast, the empty protomer reveals only water and a halide ion (Figure 1C). As shown in Figure 1B, the FAc substrate in the active site is hydrogen bonded to R111, R114, and W156 while the second substrate coordinates to the side chains of K152 (F−N: 2.9 Å) and Y141. As discussed below, K152 and Y141 are situated in a region determined to be important to allosteric communication and are both close to the backbone of a cap domain residue G252 (F−O: 3.2 Å).

Half-of-the-Sites Reactivity Is Reinforced by a Dynamic Regulatory Cap Domain. The FAcD dimer possesses a regulatory cap domain consisting of residues Ala250 to Thr259. In the substrate-free ground state the cap domains of both protomers are highly dynamic and continuous electron density is essentially missing from this regulatory region. As highlighted in Figure 2A, the cap domain appears to adopt a slightly open configuration at the entrance to the substrate binding pocket, whereas it is more closed in the

DOI: 10.1021/jacs.9b03703
J. Am. Chem. Soc. XXXX, XXX, XXX−XXX

empty protomer. Previous studies revealed that binding of substrate to one of the protomers triggers dynamics and loss of a number of tightly bound water molecules in the remaining empty protomer.[17] Thus, closure of the regulatory cap in the empty protomer prevents binding of a second substrate to this protomer, thereby ensuring the configurational entropy of the enzyme is maximally increased at a point on the reaction pathway where dynamics are needed to access subsequent functional states. At higher substrate concentrations, when a second substrate binds to an allosteric pocket in the substrate-bound protomer, the crystal structure reveals an even greater degree of change in conformation between the cap domains of the empty and occupied protomers (Figure 2B). In this case, the cap region is entirely open in the bound protomer and closes down even more in the empty protomer. Multiple molecular dynamics (MD) simulation repeats with an aggregate simulation time of 35 μs support FAc binding dependent effects on cap domain dynamics. In simulations initiated from a two-substrate/free-substrate state, cap domain dynamic fluctuations appear to become more restricted and centered around a closed configuration in the substrate-free protomer, while the cap domain of the substrate-bound protomer exhibits a wider amplitude of motions (Figure 2C). Substrate occupancy correlates with an increase in cap domain dynamics as measured by the root-mean-square fluctuations per residue (highlighted region in Figure 2D). Analysis of the distribution of cap domain conformational states sampled in the simulations reveals that substrate occupancy promotes specific conformational states of the cap domain (Figure 2E). Binding of two substrate molecules to a protomer leads to the greatest conformational heterogeneity in the cap domain, although in our simulations this state only accounted for 2 ± 1% of the data sampled. This state supports cap domain conformational states in which transient hydrogen bonds can be made with bulk substrate atoms (left protomer, Figure 2C), although the statistical significance of these interactions cannot be quantified from our data. In contrast, in the substrate-free protomer, the dynamics of the cap domain is essentially limited to small-amplitude fluctuations in a narrow, highly populated basin with a structure similar to the crystallographic state. Occupancy dependent changes to the conformational ensemble of the cap domain are visualized across multiple simulation repeats (Figure S10). The dynamics of the substrate-free cap domain may be systematically biased by the presence of the substrate-bound state in the adjacent protomer. Analysis of cap domain dynamics suggests a structural basis for the preservation of half-of-the-sites reactivity based on the modulation of cap domain fluctuations and conformational states through substrate occupancy, with causal implications for protomer allostery and substrate inhibition. This has obvious consequences with regard to interprotomer allostery, dynamic excursions of the dimer, and substrate inhibition.

High Substrate Concentrations Inhibit Catalysis. Using ^{19}F or ^{1}H NMR, it is possible to measure "real time" concentrations of substrate (FAc or ClAc, respectively) and product (F^-) in the FAcD-catalyzed reaction, as shown in Figure 3. WT-FAcD is clearly inhibited at higher substrate concentrations (for both FAc and ClAc substrates). Note that FAcD, which is optimized for fluoroacetate, hydrolyzes FAc ~10 times faster than ClAc, despite the fact that the C−F bond dissociation energy is considerably higher.[18] Crystallography suggests that inhibition is achieved through binding by a

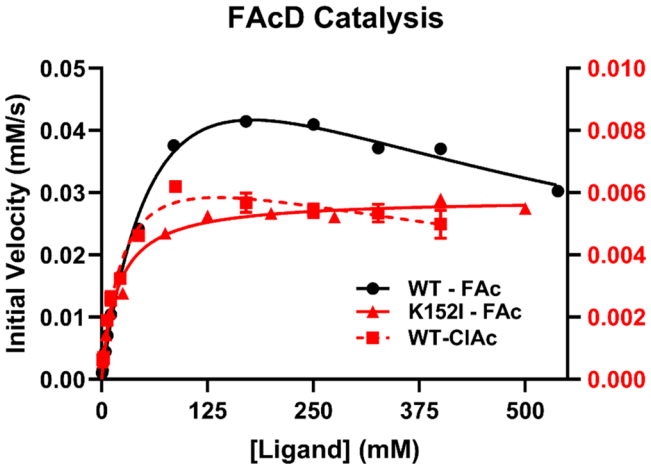

Figure 3. Enzyme kinetics of FAcD reveal substrate inhibition. Plots of initial rates as a function of substrate concentration reveal classic substrate inhibition for WT-FAcD in the presence of either FAc or ClAc substrates (shown in black and red-dashed, respectively). The mutation (K152I) results in the loss of the allosteric substrate binding pocket and thus, Michaelis−Menten kinetics as shown by the data indicated in red-solid above. Note that the reaction rate data associated with WT-FAcD, in the presence of FAc substrate, is presented using the *y*-axis scale on the left, while that for WT-FAcD with ClAc substrate or K152I with FAc substrate is graphed using the scale on the right. All data were fitted using eq 1 described in the Discussion section.

second substrate to an allosteric pocket of the substrate-bound protomer. As a control, we employed a mutant (K152I) in which a key stabilizing hydrogen bond between the epsilon amino group of the lysine side chain and the second substrate is removed. ^{15}N,^{1}H NMR spectra of K152I (Figure S2) overlap well with those of WT-FAcD, suggesting that this mutation does not significantly alter the tertiary structure or fold stability. As shown in Figure 3, the reaction rate profile of K152I FAcD now appears to follow perfect Michaelis−Menten kinetics, reaching maximal reaction rates under conditions of highest substrate concentrations (Table 1). However, this mutation also results in a loss in the rate of catalysis by over an order of magnitude. This suggests that at lower concentrations, where only one substrate is present, K152 must play a key role as a positive allosteric modulator.

FAcD binds substrate weakly and the correspondingly high off rate may be a contributing factor to low catalytic efficiency. An overall dissociation constant of the FAc substrate to the Michaelis−Menten intermediate was obtained through a ^{19}F NMR binding isotherm of FAc in the presence of the D110N mutant. The substrate affinity in the absence of the allosteric pocket (i.e., D110N/K152I) was then similarly measured. Finally, the affinity of the substrate to the allosteric pocket alone was obtained using the H280N mutant containing glycolate (covalently linked by an ester bond to the side chain of D110) in the active site. ^{19}F NMR line width analysis as a function of FAc concentration thus provides an estimate for ligand binding to the active site with k_{d1} = 0.90 ± 0.17 mM (D110N) and k_{d1} = 0.93 ± 0.11 mM for the K152I mutant, suggesting no loss of binding affinity for K152I (Table 2, Figure S3). The H280N mutant was also separately saturated with chloroacetate until the covalent intermediate was fully established. After dialysis of excess chloride and substrate, ^{19}F NMR spectra were recorded as a function of FAc substrate

DOI: 10.1021/jacs.9b03703
J. Am. Chem. Soc. XXXX, XXX, XXX−XXX

Table 1. Steady-State Kinetics of FAcD[a]

	WT-FAcD + FAc	WT-FAcD + ClAc	K152I-FAcD + FAc
V_{max} (mM/s)	8.25 ± 0.81 × 10^{-2}	8.04 ± 0.81 × 10^{-3}	5.81 ± 0.16 × 10^{-3}
K_m (mM)	86.8 ± 13.7	25.6 ± 5.6	18.8 ± 2.7
K_i (mM)	363 ± 70	727 ± 260	–
k_{cat} (s^{-1})	1.07 ± 0.11	0.106 ± 0.011	0.077 ± 0.002
k_{cat}/K_m (s^{-1} M^{-1})	12.3 ± 2.3	4.13 ± 1.00	4.12 ± 0.90

[a]The parameters were determined by fitting the data in Figure 3 with eq 1. Note that the condition used here to measure reaction kinetics (500 mM Tris buffer, pH 8.5) differ from those used in previous studies of the wild-type enzyme,[18] although the trend from FAc to ClAc is similar.

Table 2. Chemical Shift Perturbations and Line Widths of the ^{19}F NMR Peaks of One-Bound and Two-Bound States

	W156			
	CIAc	BrAc	IAc	Glycolate
CSP1 (Hz)	1060	952	731	1536
CSP2 (Hz)	908	NA	392	NA
Line Width 1 (Hz)	505	582	607	172
Line Width 2 (Hz)	264	NA	224	NA
	W185			
	CIAc	BrAc	IAc	Glycolate
CSP1 (Hz)	400	473	242	649
CSP2 (Hz)	298	NA	22	NA
Line Width 1 (Hz)	178	171	291	110
Line Width 2 (Hz)	124	NA	145	NA

concentration to determine the dissociation constant to the allosteric pocket, k_{d2}, which was estimated to be 2.2 ± 0.83 mM (Figure S3). Assuming the on rate of the second pocket is simply diffusion limited, and accounting for second-substrate affinity, the substrate off rate is expected to be on the order of 10^5 s^{-1}. Given that the catalytic rate is measured as 64.2 ± 6.6 min^{-1}, the off-rate of the second substrate is clearly not rate-limiting with regard to egress of product from the active site.

Affinity of Glycolate (Product) to the Secondary Binding Site Is Low. Crystal structures with soaking times over 24 h show the glycolate product in a new orientation, rotated by 68° and flipped. The carboxylic oxygens are still coordinated to the two arginine residues, R111 and R114, but the hydroxyl group now interacts with the halide-binding pocket instead of R114 (Figure S4). This lower energy binding orientation of glycolate in the Y219F mutant, not seen in the native protein, might well be a consequence of the loss of the tyrosine hydroxyl, leading to an altered shape and electrostatic profile of the active site. Structures determined from crystals soaked for longer than 24 h revealed only the glycolate product with no FAc species occupying the allosteric pocket. It may be that the configuration of the catalytic pocket allosterically destabilizes binding of the second substrate molecule. The lack of secondary binding in the outer pocket also suggests that the affinity of glycolate for this binding site is insufficient to lead to stable complex formation.

^{19}F NMR Shows Reduced Exchange Dynamics When Two Substrates Are Bound. We previously noted that the substrate-free enzyme undergoes millisecond time scale conformational exchange between protomers and that the frequency associated with this exchange process is in fact increased upon addition of ClAc substrate.[17] Moreover, binding of IAc, where k_{cat} is known to be slower, also results in an increase in dynamics, although to a lesser extent, suggesting that such exchange processes may facilitate sampling of key functional states required for catalysis and that the rate of such sampling may dictate the catalytic rate. Dynamics may also occur on a more localized and faster time scale. Under ideal circumstances, hints of such dynamics arise from B-factors associated with high-resolution crystal structures where regions of the empty protomer exhibit higher B-factors.[17] Binding of the second substrate to the Y219F mutant appears to restrict conformational heterogeneity of the enzyme, based on the distribution of B-factors and on electron density in regions of the protein that are observed to be dynamic in the D110N Michaelis–Menten complex. In particular, the electron density representing the cap domain is much better defined in the Y219F mutant structures (Figure 2B).

^{19}F NMR spectroscopy of 5-fluorotryptophan enriched FAcD was used to characterize the response to second-site substrate binding and inhibition with regard to the conformational ensemble and exchange dynamics. We note that in an earlier study, 5-fluorotryptophan enriched FAcD was crystallized, confirming an identical structure to that of unlabeled enzyme (root-mean-square deviation of 0.14 Å).[17] The spectra in Figure 4 and Figure S5 show the results of titration of substrates (ClAc and IAc), substrate analogue (BrAc), and product (glycolate) on ^{19}F NMR spectra of WT-FAcD. Note that for either substrate, chemical shifts and line widths associated with W156, W185, W264, and W267 shift in one direction and then reverse their trend at a concentration corresponding to where we expect to observe binding of a second substrate (Figure S6). A similar trend is seen for W185 near the active site (Figure S5). In contrast, titrations of the substrate analogue, BrAc, and product simply give rise to a monotonic trend in both chemical shift and line width, consistent with single site binding which shifts the conformational equilibrium in the enzyme.

The biphasic nature of chemical shift response to substrate binding is also observed in ^{15}N,^{1}H NMR spectra at equivalent substrate concentrations where second site binding is anticipated (Figure S7). Most of the residues that exhibit such biphasic behavior are located at the dimer interface region (Figure S7), which is in close proximity to the secondary binding site and has been previously identified as key to interprotomer allosteric communication.[17] A number of residues that are distal to the second binding site also give rise to the same biphasic behavior as shown in Figure S7A. This is also likely a consequence of long-range allosteric response to second site binding. Finally, we note that in the case of two bound substrates, specific regions in each of the protomers of the Y219F dimer crystal structure are sufficiently distinct that their corresponding amide chemical shifts are predicted (by SPARTA+) to be resolved (Figure S8). While protomer-specific resonances are not observed in either ^{19}F NMR or ^{15}N,^{1}H-HSQC (heteronuclear single quantum coherence) spectra due to fast interprotomer conformational

DOI: 10.1021/jacs.9b03703
J. Am. Chem. Soc. XXXX, XXX, XXX–XXX

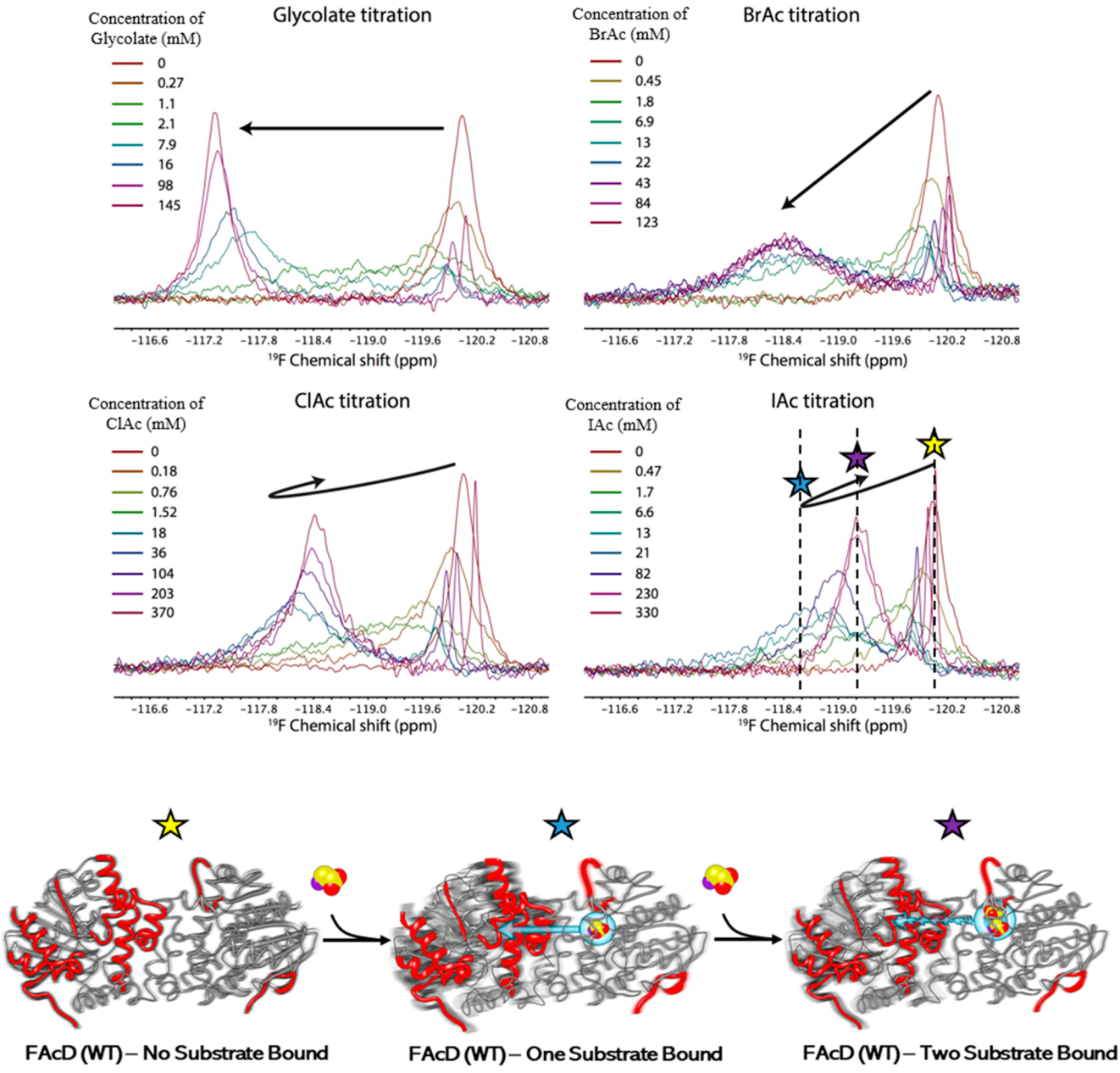

Figure 4. ^{19}F NMR spectra of W156 upon titrating product (glycolate), a substrate analog (BrAc), and substrates (ClAc and IAc) with WT-FAcD. Note that the arrows indicate the direction of the chemical shift associated with increasing ligand concentration. Shown below is an illustration of increased dynamics upon first substrate binding, followed by a dampening of dynamics upon 2nd site binding in the IAc ^{19}F NMR spectra. Blurred regions point to areas of high disorder while the red overlays indicate regions where B-factors where formerly identified as anomalously high.

exchange, we nevertheless observe a strong overlap between uniquely asymmetric regions of the dimer in the crystal structure and regions exhibiting biphasic chemical shift behavior in ^{15}N,^{1}H-HSQC spectra. Thus, while binding of two substrate molecules to the same protomer restricts overall dynamics, those regions exhibiting biphasic chemical shift perturbations likely result from a unique allosteric response (compared to that observed for single substrate binding).

Removal of the Allosteric Pocket via Deletion of a Single Amino Group Decouples the Allosteric Response to Substrate Binding in the Active Site Pocket. It is constructive to consider the relative exchange dynamics that arise in the dimer when the second site allosteric pocket is removed via the K152I mutation. Figure 5 shows a series of ^{19}F NMR spectra of 5-fluorotryptophan enriched FAcD as a function of substrate analogue (BrAc) concentration for both the WT-enzyme and the K152I mutant. BrAc exhibits poor solubility and as such, it is difficult to reach substrate concentrations needed to ensure saturation of the second binding site. We can nevertheless compare the extent of protomer conformational exchange and dynamics via the ^{19}F NMR spectra and changes in line width as a function of substrate analog. A comparison of WT-FAcD and K152I-FAcD shows there is a far weaker response in the latter, suggesting that the interprotomer conformational exchange is significantly impaired by this single mutation. Interestingly, substrate-free K152I-FAcD exhibits dynamics similar to those seen with WT-FAcD upon the addition of an equimolar amount of substrate. However, the addition of any amount of substrate analog to K152I-FAcD was shown to impair dynamics resulting in

DOI: 10.1021/jacs.9b03703
J. Am. Chem. Soc. XXXX, XXX, XXX−XXX

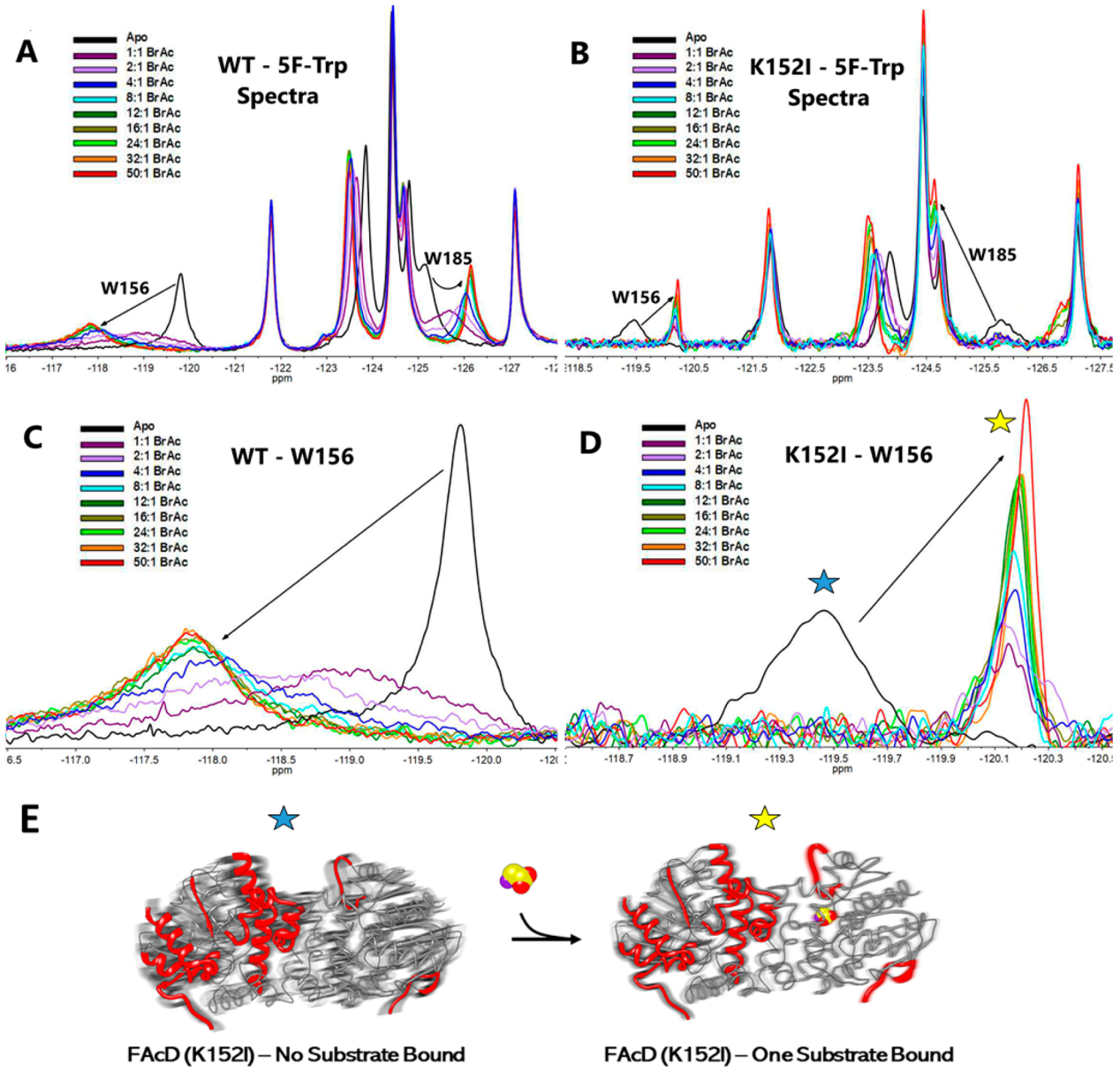

Figure 5. ^{19}F NMR spectra of 5-fluorotryptophan-enriched FAcD as a function of substrate analogue (BrAc) concentration. (A) ^{19}F NMR spectra of WT-FAcD as a function of BrAc concentration. (B) ^{19}F NMR spectra of K152I-FAcD as a function of BrAc concentration. (C) Expanded view of panel A showing change in resonances associated with W156 in the active site. (D) Expanded view of (B) showing change in resonances associated with W156 in the active site. (E) An illustration of increased dynamics in the K152I-W156 ^{19}F NMR spectra. Addition of substrate to the apo enzyme, K152I FAcD, attenuates interprotomer dynamics and shifts the conformational equilibrium to state similar to apo WT FacD.

signatures more characteristic of the substrate-free WT-FAcD. Moreover, higher amounts of BrAc resulted in a narrowing of resonances known to interface with the active site (W156 and W185), indicative of less exchange dynamics. Thus, while substrate binding to WT FAcD initiates an efficient allosteric transmission between the protomers, removal of just one amino group from the allosteric pocket results in significant attenuation of allosteric transmission upon substrate binding.

Computational Rigidity Analysis Reveals That the Second Substrate Binding Pocket Is an Allosteric Hub for Communication between Protomers. While FAcD operates via half-of-the-sites reactivity, the empty protomer plays a role in facilitating dynamics, conformational exchange, and catalysis. The pocket associated with second substrate binding is interesting from the perspective that when occupied, conformational dynamics and catalysis are simultaneously impaired, yet at lower concentrations it appears to play a key role in enhancing dynamics and catalysis. Moreover, the nonlinear ^{15}N,^{1}H chemical shift perturbations also point to extensive regions that are conformationally perturbed by second site binding, implying that there is a pronounced allosteric response associated with this site. Here, we make use of rigidity-based allosteric transmission theory to evaluate the consequences of constraining the dimer by a second substrate with regard to interprotomer allosteric transmission. Using the computational analysis previously detailed,[17] the extent of transmission of degrees of freedom (regions of flexibility or rigidity) are measured from the active site (region highlighted in green in Figure 6A) in a stepwise fashion across the entirety of the empty protomer, applying a small window of three

DOI: 10.1021/jacs.9b03703
J. Am. Chem. Soc. XXXX, XXX, XXX−XXX

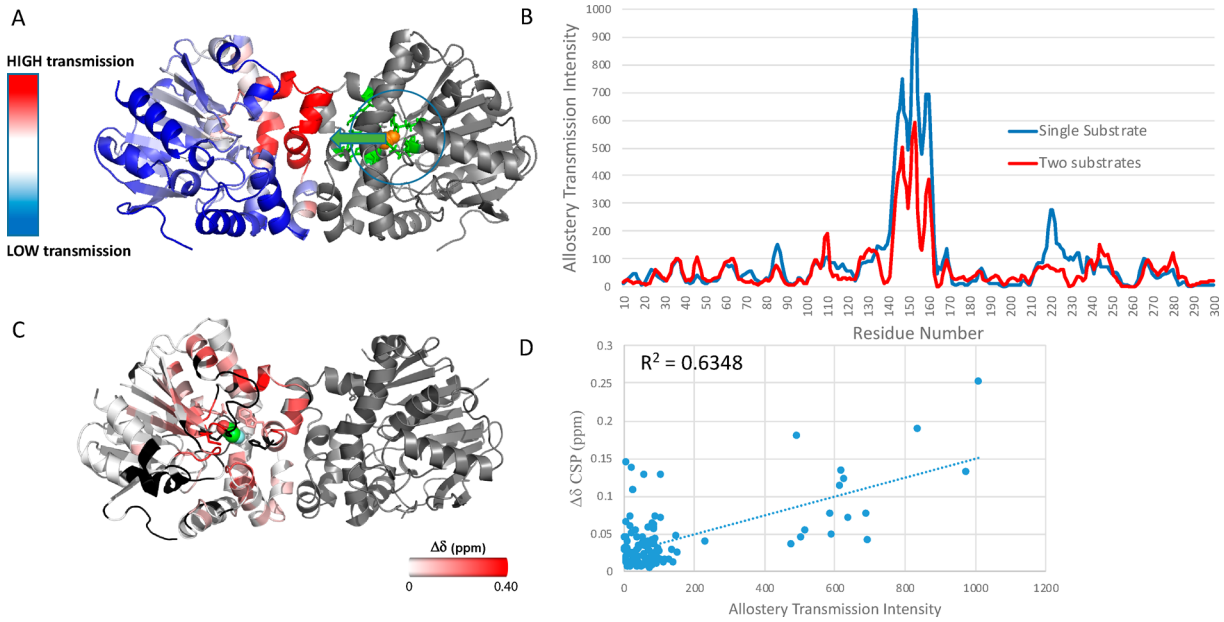

Figure 6. Computational prediction of allosteric pathway using rigidity-based allostery transmission algorithm. (A) A color map, representing the magnitude of allosteric transmission from the catalytic site of one protomer to specific regions in the empty protomer. (B) Magnitude of allosteric transmission from the catalytic site of the substrate-bound protomer to specific residues in the empty protomer, predicted from the X-ray crystal structure of the Y219F mutant with one substrate (blue) or two substrates (red) bound. (C) Chemical shift perturbations arising from binding of two substrates mapped onto the crystal structure of the substrate-bound D110N mutant. (D) Correlation between the intensity of rigidity-based allosteric transmission per residue with the corresponding $^{15}N,^{1}H$ HSQC chemical shift perturbations associated with substrate binding to the D110N mutant.

residues (Figure 6A, Figure S9). This allows us to establish an allosteric transmission intensity plot, which shows the amplitude of allosteric crosstalk between the active site of the substrate-bound protomer and the free protomer. The intensity of transmission at each residue is mapped onto the protein structure, which clearly reveals the dimer interface helix $\alpha 6$ (residues 146−160) and residues in the vicinity (i.e., residues 135−165) are crucial for interprotomer allosteric communication with the highest value occurring at I153 (Figure 6B). This region also contains residues associated with halide binding (H155, W156), the allosteric pocket (Y141, K152), and others which are adjacent to the dimer interface region. The second highest transmission peaks occur around residues 220−221, encompassing Y219 which is involved in halide binding (Figure 6B). If this analysis of allosteric transmission is repeated for the crystal structure in which two substrates are bound, the intensity of transmission is clearly reduced as shown in Figure 6B. In this case, general transmission occurs with a lower energy cutoff, more reminiscent of the apo- or product-bound states. The two bound substrate molecules inhibit the enzyme's ability to transmit allosteric change since more energy is required to transmit across the allosteric pathway. A reasonable explanation for this finding is that the underlying hydrogen bond network is stronger with the additional substrate tightening the structure.

Figure 6C indicates regions of WT-FAcD that exhibit the largest $^{15}N,^{1}H$ chemical shift perturbations upon titration of substrate analog, BrAc. These regions most likely originate from asymmetries induced in the Michaelis−Menten intermediate, that are ultimately averaged through fast interprotomer exchange. These same regions for the most part appear to overlap with regions predicted to be involved in allosteric transmission, highlighted in red in Figure 6A. The correlation between the intensity of rigidity-based allosteric transmission per residue and the residue-specific $^{15}N,^{1}H$ HSQC chemical shift perturbations is shown in Figure 6D. We also find residues in the empty protomer with very little transmission (colored in blue in Figure 6A); for instance, residues 292−300 and 195−206 exhibit limited transmission, in agreement with the lack of chemical shift perturbations seen in the $^{15}N,^{1}H$ HSQC upon titrating with BrAc.

Second Substrate-Binding Pocket Facilitates an On-Pathway Desolvation Step Prior to Substrate Binding in the Active Site. The Y219F FAcD crystal structure in the presence of a single substrate points to precise coordination of both the fluorine atom and the acetate moiety via specific hydrogen bonds (Figure 1). This begs the question as to how the substrate is first desolvated. The crystal structure of the enzyme with two substrates bound to one protomer also seems to indicate two strikingly different environments in terms of hydrophobicity. To examine the desolvation process, we first evaluated the hydrogen bond potential of the fluorine atom in organic solvent. The CH_2F moiety in the substrate has been previously suggested to serve as a stronger hydrogen bond acceptor, when compared to either CHF_2 or CF_3 moieties.[20] Titration of acetophenone, a strong hydrogen bond acceptor, to fluoroacetate in CCl_4 as shown in Figure 7A, reveals an equilibrium shift associated with hydrogen bonded waters to acetophenone at 0 °C. Note that anhydrous CCl_4 can contain up to 1.5 mM residual water.[20] Here, the equilibrium constant—and thus, the free energy—of hydrogen bonding can be measured and therefore approximated at room temperature where the enzyme kinetic measurements are performed. In the enzyme allosteric pocket, we can rely on the crystal structure associated with two bound substrates to assess hydrogen bonding via a computational docking exercise. By confining docking to the allosteric pocket, we were able to

DOI: 10.1021/jacs.9b03703
J. Am. Chem. Soc. XXXX, XXX, XXX−XXX

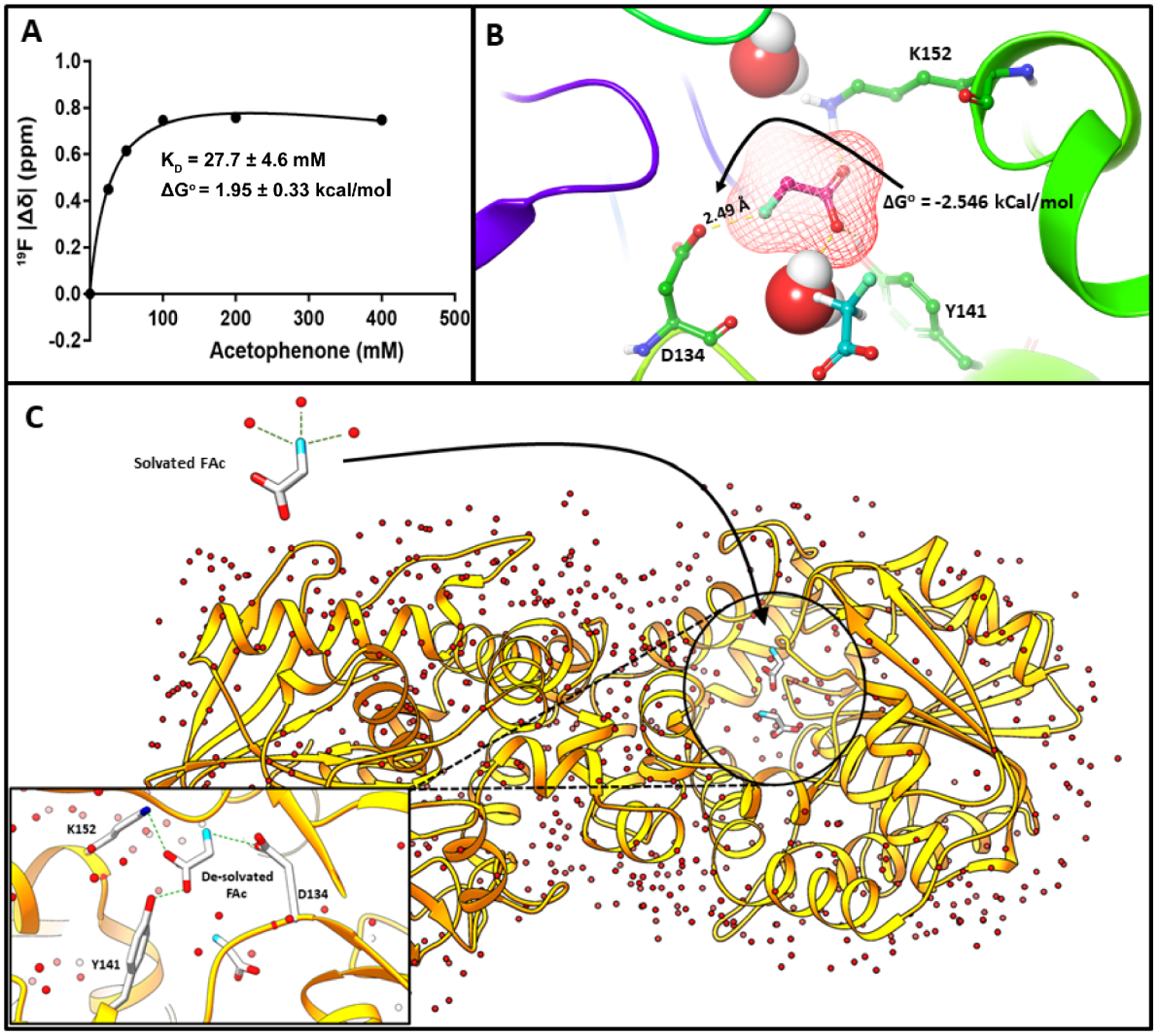

Figure 7. Hydrogen bonding to fluoroacetate in solution and desolvation of fluoroacetate in the allosteric pocket. (A) ^{19}F NMR spectra of fluoroacetate in anhydrous CCl_4 as a function of increasing amounts of acetophenone. The binding isotherm, which is performed at 0 °C to improve fidelity of detection of the hydrogen bonded complex, reveals a k_{Aeq} of 36.1 ± 6.0 mM and a corresponding free energy of 1.95 ± 0.33 kcal/mol. (B) Position of fluoroacetate in the allosteric pocket of FAcD, revealed by docking studies. The bound-state pose confirms the earlier finding by X-ray crystallography and further identifies a hydrogen bond between D134 and the fluorine atom, suggesting that substrate binding to the allosteric pocket results in desolvation of the CH_2F moiety and primes the substrate for binding to the active site. The carboxylate of D134 was predicted by PDB 2PQR (version 2.0)[22] to have a pK_a between 5.74 (apo) and 7.34 (one substrate bound). (C) Illustration of the free and allosterically bound ligand depicting desolvation of the fluorine upon binding to the allosteric site.

confirm the pose of the substrate, and at the same time identify a hydrogen bond between the fluorine atom of the substrate and the D134 side chain, as illustrated in Figure 7B. While the average pK_a of the aspartic acid side chain in folded proteins is 3.5,[21] the pK_a of D134 in the apo state of FAcD is estimated to be 5.74 and 7.34 in the Michaelis–Menten intermediate.[22] Thus, under physiological conditions, D134 would be expected to transiently adopt a protonated state, thereby enabling hydrogen bonding to FAc. Once the substrate is then deposited in the active site, the aspartate would be effectively primed to hydrogen bond to water, thereby contributing to the desolvation process. Thus, binding to the allosteric pocket likely involves a desolvation step which is key to priming the substrate for release into the active site and triggering an allosteric interprotomer response.

DISCUSSION

Half-of-the-Sites Reactivity. In this study, we have made use of the Y219F mutant of FAcD which reduces the catalytic rate to such an extent that reaction progress can be monitored by freeze-quenching crystallography. At high substrate concentrations a structure was identified in which two substrate molecules occupied one protomer along a channel connecting the protein surface to the active site, prompting us to consider the question of inhibition in the dimer. Interestingly, even under conditions where substrate concentration is in great excess, only one protomer is involved in substrate binding while the second remains empty, consistent with half-of-the-sites reactivity. Binding of substrate to one of the two protomers in the homodimer triggers an allosteric response in which the regulatory cap domain of the empty protomer is closed, blocking access of substrate. Prior X-ray crystallography studies showed that the empty protomer

DOI: 10.1021/jacs.9b03703
J. Am. Chem. Soc. XXXX, XXX, XXX−XXX

subsequently becomes more dynamic since B-factors in key distal regions of the empty protomer are then increased while ~30 bound water molecules in the same protomer are simultaneously dislodged.[17] While such a response would have key entropic advantages in terms of spurring the forward reaction, this also begs the question of the role of dynamics in catalysis since motions of the empty protomer are in turn allosterically linked to those of the substrate-bound protomer. Indeed, prior ^{19}F NMR Carr−Purcell−Meiboom−Gill (CPMG) relaxation dispersion experiments identified a 750 Hz interprotomer conformational exchange process in the apoenzyme, which increased in frequency by a factor of nearly 6 upon binding of substrate.[17] Despite the increase in interprotomer dynamics, and the increased disorder associated with the empty protomer, the cap domain effectively excludes substrate binding to the empty protomer. This can be seen by examining the conformation of the cap domain in the freeze-quenching series. Here, once a substrate is bound to one protomer, a distinctly more closed state in the other, empty protomer can be discerned. MD simulations also reveal a pronounced attenuation in cap domain dynamics associated with the empty protomer, upon binding of substrate.

Second Substrate Binding Restricts Protein Dynamics. While substrate binding increases interprotomer dynamics and disorder in the empty protomer, the addition of a second substrate to the same protomer has the opposite effect. X-ray crystallography reveals that binding of the second substrate results in unique structural changes in the cap domain and in the vicinity of helix 6 (i.e., residues 250−260 and 146−160) which become more defined in terms of electron density. B-factor distributions obtained from the series of Y219F soaked structures show reduction in local dynamics, in comparison to the B-factor distributions seen previously with the D110N mutant (Michaelis−Menten intermediate), where only one substrate is bound. The additional steric constraints imposed by binding of the second substrate also clearly influence overall dynamics. These results are echoed by ^{19}F NMR. As shown in Figure 4, we observe a prominent downfield ^{19}F NMR resonance associated with W156 upon saturation of the active site with substrate (ClAc or IAc). In this case, we make use of WT-FAcD, where the catalytic rate is sufficiently slow for the above substrates, that spectral responses can be recorded without extensive accumulation of halide product. The downfield shift seen in Figure 4 is also accompanied by significant line broadening which can be attributed to interprotomer exchange, and can be observed in ^{19}F NMR CPMG relaxation dispersions.[17] As additional substrate is added at a point where we expect second substrate binding to occur, the downfield chemical shift trend now reverses direction and the exchange-broadening decreases, indicating an attenuation of conformational exchange dynamics.

Binding of the Second Substrate Molecule Results in Allosteric Inhibition. On the basis of the crystal structure of the Y219F mutant showing two bound substrates, we propose that binding by a second substrate at an allosteric site gives rise to a ternary complex that is still able to undergo catalysis, albeit with a reduced rate constant, k_4. We can therefore describe the following sequential ordered reaction diagram[7]

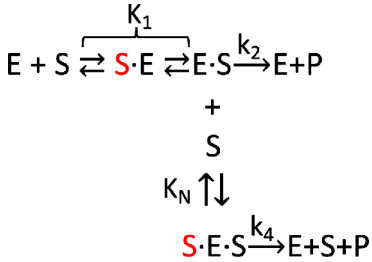

In this case, the observed initial reaction rate, V, is given by[7]

$$\frac{V}{[E_0]} = \frac{k_2[S] + k_4\frac{[S]^2}{K_i}}{K_m + \frac{[S]}{k_i K_i} + \frac{[S]^2}{K_i}} \quad (1)$$

where $[E_0]$ represents the total enzyme concentration, S·E signifies an allosteric complex in which the substrate is not in the active site pocket, E·S is the Michaelis intermediate, k_2 and k_4 are the product rate constants, K_m is the Michaelis constant, and K_i ($=1/K_N$) is the inhibition equilibrium constant. As discussed below, we hypothesize that the allosteric pocket serves as an on-pathway desolvation site and only gives rise to inhibition at very high substrate concentrations. Effectively, S·E may also be established from E, whereupon E·S is established after desolvation or the substrate disengages from the enzyme giving E+S. In the current scenario, we might expect that some of the observed inhibition may arise simply from a reduced rate of escape of product from the active site due to obstruction by substrate in the channel. However, ^{19}F NMR measurements of FAc binding to the H280N construct in which the active site is permanently occupied by a covalent intermediate reveal that the dissociation constant, k_{d2}, for second site binding is on the order of 2.2 ± 0.83 mM. The expected off rate would therefore be orders of magnitude faster than the catalytic rate, which for Y219F is on the order of min^{-1}. This leaves us with the possibility that inhibition is established exclusively by an allosteric response to second substrate binding involving both conformational and dynamic changes. Note that unlike enzymes such as phosphofructokinase and acetylcholinesterase, which become completely inhibited at high substrate concentrations,[23,24] the rate curve for FAcD does not drop to zero over the range of substrate concentrations explored. The high off rate of the second substrate may well be a contributing factor to the observed weak inhibition since the catalytic rate would then recover during periods where there is only E·S present.

Prior studies revealed that the empty protomer is a crucial part of the enzyme's catalytic machinery as it helps to compensate the entropic loss experienced by the first protomer due to substrate binding and—via interprotomer interactions—aids in the sampling of subsequent functional states needed to facilitate catalysis. In this study, we observe that stiffening by second substrate binding and the consequent attenuation of dynamics and interprotomer allostery, give rise to reduced catalysis and thus, substrate inhibition. Computational analysis of the Y219F FAcD mutant indicates an allosteric pathway, shown in Figure 6A, which runs through residues 124−165 and encompasses the allosteric pocket. The additional structural constraints and hydrogen bonds imposed by second site binding clearly raise the energy requirements for transmission of degrees of freedom and interprotomer allostery, compounding the inhibitory effect as shown in Figure 6B. Even small changes to the number of hydrogen

DOI: 10.1021/jacs.9b03703
J. Am. Chem. Soc. XXXX, XXX, XXX−XXX

bonds can have large effects on the energy requirements for transmission in FAcD. Note that the effect of the K152I mutation results in increased conformational exchange associated with the substrate-free protein, as judged by ^{19}F NMR (Figure 5C,D). However, addition of substrate greatly attenuates this exchange process resulting in a more inactive-like signature for both W156 and W185 which are in the active site. This notion of "stiffening" of the K152I enzyme upon addition of substrate is supported by predictions for the intensity of allosteric transmission (Figure 6B).

Remarkably, the above results show that removal of binding to the second pocket via the K152I mutation results in a situation where active-like signatures in the catalytic pocket are more readily sampled in the absence of substrate while inactive signatures in the catalytic pocket arise upon addition of substrate. This speaks to the role of this distal lysine (K152) as an allosteric conduit and more generally of the exquisite intra- and interprotomer allosteric networks within the enzyme which facilitate sampling of key functional states and catalysis.

Role of the Allosteric Pocket in Catalysis. Substrate inhibition is a phenomenon observed in many enzymes through a broad range of mechanisms.[7,23,25,26] Here we show for a homodimeric enzyme which acts through half-of-the-sites reactivity that catalysis is slowed upon second-site binding due primarily to restricted allosteric communication between protomers. This was quantified by rigidity theory which identified Y141 and K152 as key interprotomer allosteric hubs while also serving to bind a second substrate. Strikingly, mutation of one such residue (K152I) resulted in not only the absence of second site binding and any inhibitory effects but also a drop in V_{max} by over an order of magnitude. This suggests that the allosteric pocket may also play a role in enhancing catalysis under lower substrate concentrations, where only one substrate is anticipated to be involved in catalysis. ^{19}F NMR of fluoroacetate identified a strong hydrogen bond to the fluorine atom in organic solvent with low concentrations of residual water. Water should serve as an equally acceptable hydrogen bond donor under the aqueous conditions of enzyme action. However, docking studies suggest that FAc is desolvated in the allosteric pocket, which would then result in a more efficient transfer to the active site. Thus, the reduction in catalysis seen in the K152I mutant at low concentrations likely impairs substrate binding to the outer pocket and thus the desolvation step necessary for establishing the Michaelis–Menten intermediate and catalysis. Most importantly, upon transferring the substrate from the allosteric pocket to the active site, K152 and residues in its vicinity are predicted to play a key role in interprotomer allosteric transmission and dynamics.

Connection between Interprotomer Dynamics and Catalysis. ^{19}F NMR chemical shifts and the corresponding line widths are excellent reporters of the complex conformational equilibrium associated with FAcD and the changes which ensue upon binding of substrate or substrate analog. Briefly, the subtle asymmetries associated with side chain conformers of all nine tryptophan side chains in the apoenzyme, previously detected by X-ray crystallography, are completely averaged through millisecond time scale exchange. However, ^{19}F NMR CPMG measurements permit the study of this interprotomer exchange process. Our main conclusions from ^{19}F NMR may be thus far summarized as follows: (1) W156 appears to adopt at least 3 conformations (−120, −118.4, −117.3 ppm), with the caveat that this is averaged between two protomers in fast exchange. (2) Under apo-conditions W156 adopts a single state, which alone represents an average between two protomer conformers. Addition of substrate analog BrAc shifts the equilibrium toward a Michaelis–Menten intermediate (−118.4 ppm) though with significant broadening due only in part to the low affinity of the substrate analog. However, a significant excess of BrAc would normally be expected to reverse the effects of exchange of the BrAc substrate and shift the equilibrium to the Michaelis–Menten intermediate. Thus, the line broadening we see at saturating concentrations must be due to protein dynamics established in the Michaelis–Menten intermediate. In contrast, glycolate, which has a similar affinity to the protein as BrAc, results in exchange broadening until saturating concentrations are reached, whereupon the product-bound conformer is established. (3) The addition of substrates results in a similar broad peak as that of substrate analog, suggesting that the substrate and substrate analog both initiate significant side chain and protein dynamics at saturating concentrations. As substrate is added, the bound protomer adopts a conformation associated with the Michaelis–Menten intermediate, although interprotomer exchange is shown to increase substantially. However, the distinguishing feature of the substrates is that gross excess of substrate—where we observe substrate inhibition and simultaneous binding by two substrates—actually reduces side chain dynamics and shifts the equilibrium toward that of the substrate-free conformer.

By examining side chain orientations of W156 in the substrate-free FacD crystal structure, we note that one of the two protomers is primed for substrate binding. The crystal structure of the Michaelis–Menten intermediate shows that W156 in the empty protomer is close in orientation to that of the covalent intermediate suggesting that through protomer exchange, the covalent intermediate conformation is sampled in the active site (bound protomer). If we compare line broadening of W156 and W185 with catalytic rate measurements of ClAc, we note that there is a direct correspondence between line width and the catalytic rate. Taken together, the ^{19}F NMR data and crystallography reveal a range of distinct functional states and interprotomer exchange which facilitates exchange between functional states at the active site of the bound protomer. Dynamics play a role at every step along the reaction pathway: (1) fast dynamics likely occur in the empty protomer to compensate entropically for substrate binding, (2) cooperative dynamics connect functional states, and (3) regulatory cap dynamics preserve half-of-the-sites reactivity.

■ CONCLUSIONS AND FINAL REMARKS

In this study, we explore the mechanistic facets of substrate inhibition and interprotomer allostery associated with a homodimeric enzyme that undergoes half-of-the-sites reactivity. At very high substrate concentrations, a second substrate binds along the channel leading to the active site in the substrate-bound protomer. Spectroscopic analysis shows a decrease in the catalytic activity of the enzyme in the presence of high concentrations of substrate which coincides with a reduction in interprotomer dynamics. Rigidity-based allosteric transmission analysis points to an allosteric network, which aligns well with regions of NH-HSQC spectra exhibiting chemical shift changes through the addition of substrate. Binding of substrate to the active site is shown by rigidity analysis to enhance allosteric transmission and thus dynamics, while triggering the closing of a regulatory cap region in the

DOI: 10.1021/jacs.9b03703
J. Am. Chem. Soc. XXXX, XXX, XXX−XXX

empty protomer. Addition of a second substrate is shown by ^{19}F NMR and rigidity analysis to dampen these dynamics. Finally, analysis of enzyme kinetics in the K152I mutant, which prevents second site binding and substrate inhibition, shows a dramatic loss in the maximum catalytic rate. We therefore surmise that the allosteric substrate-binding pocket is crucial to catalysis at lower substrate concentrations, where only a single substrate engages the enzyme at one time. Our studies suggest that while the fluorine atom is stabilized by waters of hydration in the bulk phase, binding to the allosteric pocket serves to desolvate the substrate, whereupon it is deposited in the active site. As the allosteric pocket then passes off substrate to the active site it resumes its role as an allosteric hub in activating interprotomer dynamics and, consequently, catalysis. Thus, the "allosteric pocket" is likely an on-pathway desolvation site and only gives rise to inhibition at very high substrate concentrations. We note that this interprotomer allosteric conduit is only fully established once the desolvated substrate is positioned in the active site and the allosteric pocket is empty. The majority of enzymes are oligomeric. Indeed, 20% of all homodimers act through half-of-sites reactivity, which connects with the general idea of interprotomer allostery.[12,27−29] In many cases, half-of-sites reactivity is a convenient mechanism through which the active site alternates from one protomer to the other and in so doing, synchronizes the progression of multistep chemical events.[13,14,16] In this study, we can now appreciate a role for the empty protomer in catalysis and in the allosteric response that is exquisitely triggered by substrate binding.

METHODS

Expression and Purification of FAcD. FAcD from *Rhodopseudomonas palustris* was expressed in *Escherichia coli* BL21(DE3) cells and purified as published elsewhere.[17,30] For NMR experiments, cells were grown at 37 °C and induced with 1 mM isopropyl β-D-1-thiogalactopyranoside (IPTG) at an OD_{600} of 1.0−1.2 and left to express overnight. Typically, 1 g glyphosate per liter of M9 media was added to halt aromatic synthesis. Thirty minutes later, IPTG (0.24 g), tyrosine (0.075 g), 5-fluoro DL tryptophan (0.070 g), and phenylalanine (0.075 g) were added to the media. *E. coli* cells were pelleted and cell-free lysate was extracted via sonication. The lysate was loaded onto a Ni-affinity column, washed with 50 mM Tris−H_2SO_4 pH 8.5, 500 mM NaCl, 5% glycerol, 30 mM imidazole and eluted with the same buffer but with the concentration of imidazole increased to 300 mM. Cleavage of the His_6-tag was performed at room temperature overnight using TEV protease. FAcD was further purified by size exclusion chromatography (S200 16/60 HiTrap column) using 50 mM Tris−H_2SO_4, pH 8.5, 150 mM NaCl as a buffer. For storage, purified FAcD was buffer-exchanged into 50 mM Tris−H_2SO_4, pH 8.5 for several rounds to remove any remaining NaCl and then flash-frozen in liquid nitrogen.

Crystallization of FAcD. Single crystals of apo-FAcD were grown in a vapor diffusion hanging-drop set up using a 1:1 (v:v) ratio of 0.5 mM FAcD solution and a reservoir solution of 18−20% PEG3350, 200 mM $CaCl_2$, and 100 mM Tris−HCl pH 8.5. Crystals ranging from ∼200 to 500 μm in length grew after 3−5 days. To collect diffraction data for the FAc and the ClAc complexes of Y219F FAcD, crystals were soaked in artificial mother liquor in the presence of 100 mM either fluoroacetate or chloroacetate for 2 h. As FAcD crystals are catalytically active, the glycolate-complex of the Y219F mutant was obtained by soaking the crystals in mother liquor containing100 mM FAc or ClAc and leaving them to incubate for a minimum of 24 h prior to data collection.

Diffraction Data Collection. Data collection was performed at 100 K either on a Rigaku FR-E rotating anode with mirror optics and Saturn A200 detector or on a Rigaku 007 rotating copper anode with mirror optics and a Mar345 detector. Crystals were flash-frozen in liquid nitrogen using paratone N (Hampton Research, Aliso Viejo, CA, USA) as a cryo-protectant.

X-ray Data Processing and Refinement. Diffraction data were indexed, integrated, and scaled using the software package XDS.[31] Phases were calculated using the molecular replacement module of the Phaser package[32] with wild-type FAcD (PDB ID: 3R3U) as a search model. Model building and the first rounds of refinement were performed using Wincoot.[33] Automatically picked water molecules were kept for further refinement when they were within 2.3−3.5 Å of a hydrogen acceptor or donor and the corresponding electron density was at least 1.5 e/Å^3. Subsequent rounds of refinement used option Phenix.refine from the Phenix software suite.[34] Details of the crystallographic statistics and structure refinement parameters are provided in Table S1.

NMR Spectroscopy. Enzyme kinetic data were collected by acquiring either ^{19}F or ^{1}H NMR spectra for "real time" quantification of substrate (i.e., FAc or ClAc, respectively) and product (fluoride ion or glycolate) concentrations as a function of time at 25 °C. For kinetic analysis, protein concentrations were typically 75 μM using 500 mM Tris−H_2SO_4, pH 8.5 as a buffer. At these concentrations, only 16 scans were needed, encompassing 32 s per time point. The collected NMR spectra were analyzed with MestReNova (Mestrelab Research S.L., 11.0.4) and the enzyme kinetic data were fitted with a substrate inhibition model using Prism 6 (GraphPad Software).

^{19}F NMR spectra of 5-fluorotryptophan-enriched FAcD were acquired with 1600 transients and a spectral width of 22 000 Hz. The ^{19}F NMR spectra were processed and analyzed with MestReNova. ^{15}N,^{1}H HSQC spectra were typically acquired using 80 increments, 25 transients, and a spectral width of 2340 Hz in the indirect dimension. The HSQC spectra were processed with NMRPipe and NMRviewJ software. All NMR spectra were obtained on a 600 MHz Varian Inova spectrometer (Agilent technologies, Santa Clara, USA) equipped with a cryogenic probe capable of tuning to HCN or ^{19}F. ^{1}H, ^{15}N, and ^{19}F $\pi/2$ pulse widths were 10.8, 44, and 15 μs.

Enzyme binding isotherms were obtained by acquiring a series of ^{19}F NMR spectra as a function of fluoroacetate concentration, in the presence of enzyme. Protein concentrations were 100−300 μM using 500 mM Tris−H_2SO_4, pH 8.5 as a buffer. 512 scans were performed for each titration point at 30 °C. Sodium fluoride was used as an external standard in D_2O for referencing the chemical shift changes. The collected NMR spectra were analyzed with MestReNova (Mestrelab Research S.L., 11.0.4) and the enzyme binding curves were fitted with a two-site binding model using Prism 6 (GraphPad Software) to obtain a dissociation constant. H280N-FAcD was first saturated with excess ClAc overnight at room temperature to ensure all active sites were covalently occupied. Subsequent dialysis was performed to expel free Cl^- and unreacted ClAc before binding experiments were conducted with FAc.

Fluoroacetate hydrogen bonding was studied by monitoring the ^{19}F NMR chemical shift of FAc as a function of the concentration of the hydrogen bond acceptor, acetophenone, in CCl_4, using an external reference (trifluoro-toluene). CCl_4 contains trace amounts of H_2O which would serve as the hydrogen bond donor and acetophenone would then compete with $-CH_2F$ for these waters of hydration. Acetophenone was titrated (into 5 mM FAc) from 25 to 400 mM. The change in the chemical shift of FAc in reference to trifluoro-toluene was plotted against increasing concentration of acetophenone, as described elsewhere.[20,35]

Molecular Dynamics Methods. Molecular models for simulations were constructed using the substrate-bound Y219F structure of FAcD (PDB: 6QKW). Missing residues were modeled at the N-terminus of chain C, and the Y219F mutation was reverted to obtain a dimer of the full-length wild-type sequence (numbered as residues −1 to 300).[36] All titratable residues and termini were in the standard protonation state for simulations at pH 7. Bound FAc substrate, chloride ion, and water molecules were preserved in their crystallographic position in all molecular models. Four systems were constructed with increasing concentrations of FAc in solution, resulting in simulation cells with 2, 14, 50, and 100 FAc molecules

DOI: 10.1021/jacs.9b03703
J. Am. Chem. Soc. XXXX, XXX, XXX−XXX

(including the FAcD bound substrate). The final rhombic dodecahedron simulation cell consisted of the protein dimer, ~28 000 water molecules, 136 Na^+, and the required number of Cl^- to neutralize the system cell. The protein was modeled with the amber99sb-ildn force field[37] with TIP3P[38] water. AMBER compatible parameters for fluoroacetate were generated using the acpype/Antechamber[39,40] parametrization protocol resulting in the following partial charges; CT 0.116700, C 0.877602, O2−0.835501, F −0.304700, H1 −0.009300.

All minimization, equilibration, and production simulations were conducted using GROMACS 4.6.5[41] where all molecular dynamics was performed with a time step of 2 fs. Each system was subjected to 2000 steps of steepest descent energy minimization to remove unfavorable energy contacts. Equilibration was performed in two successive blocks of simulation length 5 ns in the NVT and NPT statistical ensembles, where protein and FAc heavy-atoms were restrained with a force constant of 1000 and 500 kJ mol^{-1} nm^{-1}, respectively. For production simulations, five separate simulation repeats were constructed for the "2 FAc" system, and ten separate simulation repeats were constructed for all other systems ("14 FAc", "50 FAc", and "100 FAc"), with randomized initial velocities of all atoms at a temperature of 300 K. The position of FAc in solution was also randomized for each simulation repeat. These simulations were performed in the NPT ensemble at a temperature of 300 K with the Nosé−Hoover thermostat[42,43] (collision frequency of 0.5 ps^{-1}) and at a pressure of 1 atm using the Parrinello−Rahman barostat[44] (coupling constant of 2 ps). Lennard-Jones interactions were evaluated using a group-based cutoff for separation distances of 1.2 nm. Coulomb interactions were calculated using the smooth particle-mesh Ewald method[45,46] with a real-space cutoff of 1.2 nm and a Fourier grid spacing of 0.16 nm. The nonbonded pair-list was updated every 10 fs. All covalent bonds were constrained with SETTLE[47] and P-LINCS[48] for water and other molecules, respectively. Each simulation repeat was run for 1000 ns, for an aggregate total of 35 μs. All production data before 50 ns were discarded from each replica to account for equilibration.

For data analysis, all dimers were separated into monomers and data for all monomer occupancy states were pooled together and subsampled at a time interval of 1 ns. Monomer binding site occupancy was determined by computing the average distance of each FAc molecule C atom to the C-α atom of several amino acids that line the binding pocket (defined as residues 114, 110, 135, 136, 141, and 156). Active site occupancy was defined with an average distance below the cutoff of 1.2 nm, defined on the basis of the first minima in the radial distribution function. For the computation of root-mean-square fluctuations and root-mean-square deviations, monomers were first aligned to a reference structure determined from X-ray crystallography using all C-α atoms greater than residue 7. Fluctuations were measured after aligning the structure to the unoccupied monomer from the original structural model (originally derived from the Y219F structure). Subsequent root-mean-square deviation calculations were made with respect to the unoccupied monomer as well as the "two substrate"-bound monomer using all C-alpha atoms of the cap domain (residues 250 to 259). Analysis was performed using MDTraj[49] and all molecular renderings of crystallographic structures and MD snapshots in Figure 2 were generated using VMD.[50] The molecular rendering in panel 2A was generated using the crystal structure of D110N/FAc cocrystal structure (PDB: 5SWN) where a single missing residue in the cap domain (chain A, A257) was modeled, energy minimized, and briefly simulated using the protein preparation protocol in the Schrödinger Maestro 11.6.013 software.[51,52]

Computational Prediction of Allosteric Pathways. *Rigidity-Based Allosteric Communication.* To quantify the allosteric effect and map out the allosteric pathway between the substrate binding region in one protomer and the other protomer, we applied a rigidity-transmission allostery (RTA) algorithm. This computational method was introduced in 2012[53] and is based upon rigidity theory[54,55] and utilizes extensions of the program FIRST.[56−58] The RTA algorithm measures the effect of local mechanical propagation of rigidity across (distant) parts of the protein structure.[17] In this work, we analyzed how the perturbation of rigidity of the catalytic site is transmitted to the second protomer both in the presence and absence of a critical mutation (K152I) lying in the allosteric pocket.

Starting with an X-ray crystal structure, FIRST generates a constraint network, where the protein is modeled in terms of nodes (atoms) and edges (i.e., constraints representing covalent bonds, hydrogen bonds, electrostatic interactions, and hydrophobic contacts). Hydrogen bonds are ranked in terms of overall strength using the modified Mayo potential,[57] whereupon a hydrogen bond cutoff energy value is selected such that all bonds weaker than this cutoff are ignored. FIRST applies the pebble game algorithm,[56] which rapidly decomposes a resulting network into rigid clusters and flexible regions, enabling an evaluation of nontrivial degrees of freedom (DOF) throughout the protein. After generating outputs of the pebble game algorithm (FIRST) at a wide range of energy cutoffs, we applied the RTA algorithm to predict if local perturbation of rigidity at one catalytic site (mimicking ligand/substrate binding) propagates across the protein network and leads to a change in rigidity and the number of conformational degrees of freedom in the regions of the other protomer, hence resulting in allosteric transmission. Equivalently, the presence of rigidity-based allostery means that a change in shape (conformation) at the catalytic site (i.e., mechanically changing the shape as binding might) would lead to rearrangement and change of the shape in parts of the other protomer. Utilizing the RTA algorithm, prediction of allosteric response for each residue in the empty protomer is calculated following rigidity perturbation of the catalytic site, enabling us to obtain a detailed map of the allosteric network between the two protomers.

We used FIRST and the pebble game algorithm to compute conformational degrees of freedom for all small windows consisting of three consecutive residues in the empty protomer, before and after a perturbation of rigidity of the catalytic site. The residues in the empty monomer that undergo a change in internal degrees of freedom (i.e., propagation of rigidity-transmission of degrees of freedom) upon rigidity perturbation of the catalytic site form the allosteric pathway connecting the two protomers. Residues in Figure 6A are color-coded based on the amount of transmission of degrees of freedom.

Computation of Rigidity-Transmission Allostery (RTA). Missing hydrogen atoms were added to crystal structures with the WHAT IF web server (http://swift.cmbi.ru.nl/servers/html/htopo.html). For every hydrogen bond energy cutoff, starting at 0 kcal/mol (the cutoff is lowered in increments of 0.01 kcal/mol), the FIRST method (as previously described) was performed to generate the output of rigidity prediction and the pebble game algorithm.

We compute the number of degrees of freedom that can be transmitted (removed) from a window of 3 consecutive residues (r, r + 2) in the empty monomer as a result of perturbation of the rigidity of the substrate-binding region (residues 110, 111, 114, 141, 155, 156, 185, and 219). Starting at the N-terminal end of the empty protomer, beginning with window (1, 3), then (2,4), etc., continuing to slide the window of 3 consecutive residues, we computed the transmission of degrees of freedom for every window. Initial perturbation of rigidity refers to insertion of additional constraints (edges) (removal of degrees of freedom) to the substrate-binding region up to its rigidification. When transmission of degrees of freedom occurs, it refers to any subsequent change in the number of degrees of freedom at the (distant) window in the empty protomer.

Transmission of degrees of freedom between the two sites was computed with the aid of the pebble game. Let the substrate binding region be denoted as site A and the current tested window as site B, and for every energy cutoff we calculate the available conformational degrees of freedom at site A, site B and the union of sites A and B. Using the output of the pebble game (FIRST), degrees of freedom counts were computed by calculating the maximum number of pebbles that could be gathered on nodes (atoms) belonging to site A, site B and finally the union of sites A and B. Given some fixed energy cutoff, we denoted these counts as A_{DOF}, B_{DOF}, and AB_{DOF}, respectively. In the pebble game algorithm, each pebble corresponds to a degree of freedom. The maximum number of degrees of freedom

DOI: 10.1021/jacs.9b03703
J. Am. Chem. Soc. XXXX, XXX, XXX−XXX

that can be transmitted from A to B (denoted as DOF_AB) was finally calculated by obtaining the count DOF_AB = A_{DOF} + B_{DOF} − AB_{DOF} − 6. Six was subtracted to neglect the trivial six degrees of freedom corresponding to rigid body motions. When DOF_AB was positive, then sites A and B were involved in rigidity-based allosteric transmission and the maximum number of degrees of freedom that can be transmitted from A to B is DOF_AB. This provided a quantifiable measure of allosteric communication between A and B. To observe allosteric transmission for some residue *r*, a transmission of degrees of freedom curve was generated by plotting the averaged DOF_AB for three consecutive windows containing *r* (i.e., (*r* − 2, *r*), (*r* − 1, *r* + 1) and (*r*, *r* + 2)) as a function of the energy cutoff. We calculated the intensity of allosteric transmission for each window of 3 consecutive residues by computing the area under the transmission of degrees of freedom curve. The intensity of allosteric transmission for residue r was obtained by calculating the average intensity of the three consecutive windows that contain the residue *r* (Figure 6A,B). The intensity of allosteric transmission took into account the number of degrees of freedom that can be transmitted but also the persistence of the transmission as a function of energy strength.

Docking Studies. All described *in silico* experiments were performed on the Schrödinger Maestro 11.6.013 software using Glide within the Small-Molecule Drug Discovery Suite 2018-4 (Schrödinger, LLC, New York, NY,2018).[51,52] These studies required the following programs within the above suite: Epik, Optimized Potentials for Liquid Simulations 3e (OPLS3e) force-field, Glide, LigPrep, and the Protein Preparation Wizard. Other softwares used include ChemDraw Professional 17.1. All ligand poses and protein structure images were generated with Maestro 11.6. The chemical structure of fluoroacetate was drawn into Maestro 11.6.013 before undergoing a ligand preparation workflow (LigPrep, Schrödinger, LLC, New York, NY, 2018) using the OPLS3eforce-field. This involved ionization using Epik to generate possible protonation states at target pH 7.0 ± 2.0, desalting and generating tautomers (if applicable). The compound was then energetically minimized and the resulting 3-dimensional structure used to specify chiral centers. The prepared fluoroacetate small molecule was screened against FAcD, within a 10 × 10 × 10 Å cube using the Standard Precision (SP) docking workflow. The top 30 binding poses were generated and ranked as a function of docking score (kcal mol^{-1}).

■ ASSOCIATED CONTENT

Supporting Information

The Supporting Information is available free of charge on the ACS Publications website at DOI: 10.1021/jacs.9b03703.

Statistics of crystallographic data collection and structure refinement, 2Fo-Fc electron density map of the active site of Y219F at various points of the catalytic cycle, overlay of ^{15}N,^{1}H NMR spectra of apo-WT-FAcD (black) and apo-K152I (red), ^{19}F NMR binding isotherms, product glycolate bound to the active site in the Y219F mutant after a 24 h soak, ^{19}F NMR spectra of 5F-Trp-enriched FAcD titrated with different ligands, ^{19}F NMR chemical shift changes of W156 as a function of ligand concentration for D110N FAcD, 15N,1H HSQC spectra of FAcD as a function of ClAc concentration, SPARTA+ analysis of differences between soaked Y219F and wild-type structures, degree of freedom transmission calculations for different transmission regions, molecular rendering of regulatory cap domain fluctuations from molecular dynamics simulations. (PDF)

■ AUTHOR INFORMATION

Corresponding Authors

*scott.prosser@utoronto.ca

*emil.pai@utoronto.ca

ORCID

Pedram Mehrabi: 0000-0003-3211-6959

Emil F. Pai: 0000-0002-1162-7242

R. Scott Prosser: 0000-0001-9351-178X

Author Contributions

▽These authors contributed equally to this work.

Author Contributions

¶The contributions by these authors are of equal importance.

Notes

The authors declare no competing financial interest.

■ ACKNOWLEDGMENTS

We thank A. Dong (Structural Genomics Consortium, Toronto) for his help with collecting X-ray diffraction data. We also thank Yasir Raouf for assistance in docking studies. This work was supported by the Canadian Institutes of Health Research Training Program in Protein Folding and Interaction Dynamics and an Ontario Graduate Scholarship (T.H.K.), an Ontario Student Opportunity Trust Fund award (P.M.), CREST/JST (A.S.), Natural Sciences and Engineering Research Council of Canada Discovery grants 418679 (R.S.P.) and RGPIN-2015-04877 (E.F.P.), Canadian Institutes of Health Research grant MOP-130461 (R.P.), and the Canada Research Chairs Program (E.F.P.). Molecular dynamics computations were performed on the GPC supercomputer at the SciNet HPC Consortium. SciNet is funded by the Canada Foundation for Innovation under the auspices of Compute Canada, the Government of Ontario, Ontario Research Fund−Research Excellence, and the University of Toronto. Coordinates and structure factors have been deposited in the Protein Data Bank with accession numbers 6QKS, 6QKW, 6QKT, and 6QKU for the apo-form of the Y219F mutant of FAcD, the Y219F-FAc-complex, the Y219F-glycolate complex, and the Y219F-ClAc complex, respectively.

■ REFERENCES

(1) Tawfik, D. S. Accuracy-Rate Tradeoffs: How Do Enzymes Meet Demands of Selectivity and Catalytic Efficiency? *Curr. Opin. Chem. Biol.* **2014**, *21*, 73−80.

(2) Eisenmesser, E. Z.; Millet, O.; Labeikovsky, W.; Korzhnev, D. M.; Wolf-Watz, M.; Bosco, D. A.; Skalicky, J. J.; Kay, L. E.; Kern, D. Intrinsic Dynamics of an Enzyme Underlies Catalysis. *Nature* **2005**, *438* (7064), 117−121.

(3) Boehr, D. D.; Dyson, H. J.; Wright, P. E. An NMR Perspective on Enzyme Dynamics. *Chem. Rev.* **2006**, *106* (8), 3055−3079.

(4) Henzler-Wildman, K. A.; Thai, V.; Lei, M.; Ott, M.; Wolf-Watz, M.; Fenn, T.; Pozharski, E.; Wilson, M. A.; Petsko, G. A.; Karplus, M.; Hübner, C. G.; Kern, D. Intrinsic Motions Along an Enzymatic Reaction Trajectory. *Nature* **2007**, *450* (7171), 838−844.

(5) Tzeng, S.-R.; Kalodimos, C. G. Protein Dynamics and Allostery: an NMR View. *Curr. Opin. Struct. Biol.* **2011**, *21* (1), 62−67.

(6) Guo, J.; Zhou, H.-X. Protein Allostery and Conformational Dynamics. *Chem. Rev.* **2016**, *116* (11), 6503−6515.

(7) Reed, M. C.; Lieb, A.; Nijhout, H. F. The Biological Significance of Substrate Inhibition: a Mechanism with Diverse Functions. *BioEssays* **2010**, *32* (5), 422−429.

(8) Colletier, J.-P.; Fournier, D.; Greenblatt, H. M.; Stojan, J.; Sussman, J. L.; Zaccai, G.; Silman, I.; Weik, M. Structural Insights Into Substrate Traffic and Inhibition in Acetylcholinesterase. *EMBO J.* **2006**, *25* (12), 2746−2756.

(9) Dolenc, I.; Turk, B.; Pungercic, G.; Ritonja, A.; Turk, V. Oligomeric Structure and Substrate-Induced Inhibition of Human Cathepsin-C. *J. Biol. Chem.* **1995**, *270* (37), 21626−21631.

DOI: 10.1021/jacs.9b03703
J. Am. Chem. Soc. XXXX, XXX, XXX−XXX

(10) Sekulic, N.; Konrad, M.; Lavie, A. Structural Mechanism for Substrate Inhibition of the Adenosine 5′-Phosphosulfate Kinase Domain of Human 3′-Phosphoadenosine 5′-Phosphosulfate Synthetase 1 and Its Ramifications for Enzyme Regulation. *J. Biol. Chem.* **2007**, *282* (30), 22112−22121.
(11) Chen, C.; Joo, J. C.; Brown, G.; Stolnikova, E.; Halavaty, A. S.; Savchenko, A.; Anderson, W. F.; Yakunin, A. F. Structure-Based Mutational Studies of Substrate Inhibition of Betaine Aldehyde Dehydrogenase BetB From Staphylococcus Aureus. *Appl. Environ. Microbiol.* **2014**, *80* (13), 3992−4002.
(12) Levitzki, A.; Stallcup, W. B.; Koshland, D. E. Half-of-the-Sites Reactivity and the Conformational States of Cytidine Triphosphate Synthetase. *Biochemistry* **1971**, *10* (18), 3371−3378.
(13) Frank, R.; Titman, C. M.; Pratap, J. V.; Luisi, B. F.; Perham, R. N. A Molecular Switch and Proton Wire Synchronize the Active Sites in Thiamine Enzymes. *Science* **2004**, *306* (5697), 872−876.
(14) Seifert, F.; Golbik, R.; Brauer, J.; Lilie, H.; Schröder-Tittmann, K.; Hinze, E.; Korotchkina, L. G.; Patel, M. S.; Tittmann, K. Direct Kinetic Evidence for Half-of-the-Sites Reactivity in the E1 Component of the Human Pyruvate Dehydrogenase Multienzyme Complex Through Alternating Sites Cofactor Activation †. *Biochemistry* **2006**, *45* (42), 12775−12785.
(15) Castellani, M.; Covian, R.; Kleinschroth, T.; Anderka, O.; Ludwig, B.; Trumpower, B. L. Direct Demonstration of Half-of-the-Sites Reactivity in the Dimeric Cytochrome Bc1 Complex: Enzyme with One Inactive Monomer Is Fully Active but Unable to Activate the Second Ubiquinol Oxidation Site in Response to Ligand Binding at the Ubiquinone Reduction Site. *J. Biol. Chem.* **2010**, *285* (1), 502−510.
(16) Schröder-Tittmann, K.; Meyer, D.; Arens, J.; Wechsler, C.; Tietzel, M.; Golbik, R.; Tittmann, K. Alternating Sites Reactivity Is a Common Feature of Thiamin Diphosphate-Dependent Enzymes as Evidenced by Isothermal Titration Calorimetry Studies of Substrate Binding. *Biochemistry* **2013**, *52* (15), 2505−2507.
(17) Kim, T. H.; Mehrabi, P.; Ren, Z.; Sljoka, A.; Ing, C.; Bezginov, A.; Ye, L.; Pomès, R.; Prosser, R. S.; Pai, E. F. The Role of Dimer Asymmetry and Protomer Dynamics in Enzyme Catalysis. *Science* **2017**, *355* (6322), No. eaag2355.
(18) Chan, P. W. Y.; Yakunin, A. F.; Edwards, E. A.; Pai, E. F. Mapping the Reaction Coordinates of Enzymatic Defluorination. *J. Am. Chem. Soc.* **2011**, *133* (19), 7461−7468.
(19) Fiedler, E.; Thorell, S.; Sandalova, T.; Golbik, R.; König, S.; Schneider, G. Snapshot of a Key Intermediate in Enzymatic Thiamin Catalysis: Crystal Structure of the Alpha-Carbanion of (Alpha, Beta-Dihydroxyethyl)-Thiamin Diphosphate in the Active Site of Transketolase From Saccharomyces Cerevisiae. *Proc. Natl. Acad. Sci. U. S. A.* **2002**, *99* (2), 591−595.
(20) Dalvit, C.; Invernizzi, C.; Vulpetti, A. Fluorine as a Hydrogen-Bond Acceptor: Experimental Evidence and Computational Calculations. *Chem. - Eur. J.* **2014**, *20* (35), 11058−11068.
(21) Grimsley, G. R.; Scholtz, J. M.; Pace, C. N. A Summary of the Measured pK Values of the Ionizable Groups in Folded Proteins. *Protein Sci.* **2009**, *18* (1), 247−251.
(22) Dolinsky, T. J.; Nielsen, J. E.; McCammon, J. A.; Baker, N. A. PDB2PQR: an Automated Pipeline for the Setup of Poisson-Boltzmann Electrostatics Calculations. *Nucleic Acids Res.* **2004**, *32*, W665−W667.
(23) Fenton, A. W.; Reinhart, G. D. Mechanism of Substrate Inhibition in Escherichia Coli Phosphofructokinase. *Biochemistry* **2003**, *42* (43), 12676−12681.
(24) Shafferman, A.; Velan, B.; Ordentlich, A.; Kronman, C.; Leitner, M.; Grosfeld, H.; Flashner, Y.; Cohen, S.; Barak, D.; Ariel, N. Substrate-Inhibition of Acetylcholinesterase - Residues Affecting Signal Transduction From the Surface to the Catalytic Center. *EMBO J.* **1992**, *11* (10), 3561−3568.
(25) McLoughlin, S. Y.; Ollis, D. L. The Role of Inhibition in Enzyme Evolution. *Chem. Biol.* **2004**, *11* (6), 735−737.
(26) Wu, B. Substrate Inhibition Kinetics in Drug Metabolism Reactions. *Drug Metab. Rev.* **2011**, *43* (4), 440−456.
(27) Hill, T. L.; Levitzki, A. Subunit Neighbor Interactions in Enzyme-Kinetics - Half-of-the-Sites Reactivity in a Dimer. *Proc. Natl. Acad. Sci. U. S. A.* **1980**, *77* (10), 5741−5745.
(28) Kornev, A. P.; Taylor, S. S. Dynamics-Driven Allostery in Protein Kinases. *Trends Biochem. Sci.* **2015**, *40* (11), 628−647.
(29) Kim, J.; Ahuja, L. G.; Chao, F.-A.; Xia, Y.; McClendon, C. L.; Kornev, A. P.; Taylor, S. S.; Veglia, G. A Dynamic Hydrophobic Core Orchestrates Allostery in Protein Kinases. *Sci. Adv.* **2017**, *3* (4), No. e1600663.
(30) Chan, W. Y.; Wong, M.; Guthrie, J.; Savchenko, A. V.; Yakunin, A. F.; Pai, E. F.; Edwards, E. A. Sequence- and Activity-Based Screening of Microbial Genomes for Novel Dehalogenases. *Microb. Biotechnol.* **2010**, *3* (1), 107−120.
(31) Kabsch, W. XDS. *Acta Crystallogr. D Biol. Crystallogr.* **2010**, *66* (Pt 2), 125−132.
(32) McCoy, A. J.; Grosse-Kunstleve, R. W.; Adams, P. D.; Winn, M. D.; Storoni, L. C.; Read, R. J. Phaser Crystallographic Software. *J. Appl. Crystallogr.* **2007**, *40* (Pt 4), 658−674.
(33) Emsley, P.; Lohkamp, B.; Scott, W. G.; Cowtan, K. Features and Development of Coot. *Acta Crystallogr. D Biol. Crystallogr.* **2010**, *66* (Pt 4), 486−501.
(34) Adams, P. D.; Afonine, P. V.; Bunkóczi, G.; Chen, V. B.; Davis, I. W.; Echols, N.; Headd, J. J.; Hung, L.-W.; Kapral, G. J.; Grosse-Kunstleve, R. W.; McCoy, A. J.; Moriarty, N. W.; Oeffner, R.; Read, R. J.; Richardson, D. C.; Richardson, J. S.; Terwilliger, T. C.; Zwart, P. H. PHENIX: A Comprehensive Python-Based System for Macromolecular Structure Solution. *Acta Crystallogr. D Biol. Crystallogr.* **2010**, *66* (Pt 2), 213−221.
(35) Dalvit, C.; Vulpetti, A. Weak Intermolecular Hydrogen Bonds with Fluorine: Detection and Implications for Enzymatic/Chemical Reactions, Chemical Properties, and Ligand/Protein Fluorine NMR Screening. *Chem.—Eur. J.* **2016**, *22*, 7592−7601.
(36) Fiser, A.; Sali, A. MODELLER: Generation and Refinement of Homology-Based Protein Structure Models. *Methods Enzymol.* **2003**, *374*, 461−491.
(37) Lindorff-Larsen, K.; Piana, S.; Palmo, K.; Maragakis, P.; Klepeis, J. L.; Dror, R. O.; Shaw, D. E. Improved Side-Chain Torsion Potentials for the Amber ff99SB Protein Force Field. *Proteins: Struct., Funct., Genet.* **2010**, *19*, NA−NA.
(38) Jorgensen, W. L.; Chandrasekhar, J.; Madura, J. D.; Impey, R. W.; Klein, M. L. Comparison of Simple Potential Functions for Simulating Liquid Water. *J. Chem. Phys.* **1983**, *79* (2), 926−935.
(39) Sousa da Silva, A. W.; Vranken, W. F. ACPYPE - AnteChamber PYthon Parser interfacE. *BMC Res. Notes* **2012**, *5* (1), 367−369.
(40) Wang, J.; Wang, W.; Kollman, P. A.; Case, D. A. Automatic Atom Type and Bond Type Perception in Molecular Mechanical Calculations. *J. Mol. Graphics Modell.* **2006**, *25* (2), 247−260.
(41) Pronk, S.; Páll, S.; Schulz, R.; Larsson, P.; Bjelkmar, P.; Apostolov, R.; Shirts, M. R.; Smith, J. C.; Kasson, P. M.; van der Spoel, D.; Hess, B.; Lindahl, E. GROMACS 4.5: A High-Throughput and Highly Parallel Open Source Molecular Simulation Toolkit. *Bioinformatics* **2013**, *29* (7), 845−854.
(42) Hoover, W. G. Canonical Dynamics - Equilibrium Phase-Space Distributions. *Phys. Rev. A: At., Mol., Opt. Phys.* **1985**, *31* (3), 1695−1697.
(43) Nosé, S. A Unified Formulation of the Constant Temperature Molecular Dynamics Methods. *J. Chem. Phys.* **1984**, *81* (1), 511−519.
(44) Nosé, S.; Klein, M. L. Constant Pressure Molecular Dynamics for Molecular Systems. *Mol. Phys.* **1983**, *50* (5), 1055−1076.
(45) Darden, T.; York, D.; Pedersen, L. Particle Mesh Ewald: an N·Log(N) Method for Ewald Sums in Large Systems. *J. Chem. Phys.* **1993**, *98* (12), 10089−10092.
(46) Essmann, U.; Perera, L.; Berkowitz, M. L.; Darden, T.; Lee, H.; Pedersen, L. G. A Smooth Particle Mesh Ewald Method. *J. Chem. Phys.* **1995**, *103* (19), 8577−8593.
(47) Miyamoto, S.; Kollman, P. A. Settle - an Analytical Version of the Shake and Rattle Algorithm for Rigid Water Models. *J. Comput. Chem.* **1992**, *13* (8), 952−962.

DOI: 10.1021/jacs.9b03703
J. Am. Chem. Soc. XXXX, XXX, XXX−XXX

(48) Hess, B. P-LINCS: a Parallel Linear Constraint Solver for Molecular Simulation. *J. Chem. Theory Comput.* **2008**, *4* (1), 116−122.
(49) McGibbon, R. T.; Beauchamp, K. A.; Harrigan, M. P.; Klein, C.; Swails, J. M.; Hernández, C. X.; Schwantes, C. R.; Wang, L.-P.; Lane, T. J.; Pande, V. S. MDTraj: a Modern Open Library for the Analysis of Molecular Dynamics Trajectories. *Biophys. J.* **2015**, *109* (8), 1528−1532.
(50) Humphrey, W.; Dalke, A.; Schulten, K. VMD: Visual Molecular Dynamics. *J. Mol. Graphics* **1996**, *14* (1), 33−38.
(51) Friesner, R. A.; Banks, J. L.; Murphy, R. B.; Halgren, T. A.; Klicic, J. J.; Mainz, D. T.; Repasky, M. P.; Knoll, E. H.; Shelley, M.; Perry, J. K.; Shaw, D. E.; Francis, P.; Shenkin, P. S. Glide: A New Approach for Rapid, Accurate Docking and Scoring. 1. Method and Assessment of Docking Accuracy. *J. Med. Chem.* **2004**, *47* (7), 1739−1749.
(52) Friesner, R. A.; Murphy, R. B.; Repasky, M. P.; Frye, L. L.; Greenwood, J. R.; Halgren, T. A.; Sanschagrin, P. C.; Mainz, D. T. Extra Precision Glide: Docking and Scoring Incorporating a Model of Hydrophobic Enclosure for Protein-Ligand Complexes. *J. Med. Chem.* **2006**, *49* (21), 6177−6196.
(53) Sljoka, A. *Algorithms in Rigidity Theory with Applications to Protein Flexibility and Mechanical Linkages*. Ph.D. Dissertation, York University, Toronto, Ontario, Canada, August 2012.
(54) Whiteley, W. Counting Out to the Flexibility of Molecules. *Phys. Biol.* **2005**, *2* (4), S116−S126.
(55) Finbow-Singh, W.; Whiteley, W. Isostatic Block and Hole Frameworks. *SIAM Journal on Discrete Mathematics* **2013**, *27* (2), 991−1020.
(56) Jacobs, D. J.; Hendrickson, B. An Algorithm for Two-Dimensional Rigidity Percolation: The Pebble Game. *J. Comput. Phys.* **1997**, *137* (2), 346−365.
(57) Jacobs, D. J.; Rader, A. J.; Kuhn, L. A.; Thorpe, M. F. Protein Flexibility Predictions Using Graph Theory. *Proteins: Struct., Funct., Genet.* **2001**, *44* (2), 150−165.
(58) Chubynsky, M. V.; Thorpe, M. F. Algorithms for Three-Dimensional Rigidity Analysis and a First-Order Percolation Transition. *Phys. Rev. E Stat Nonlin Soft Matter Phys.* **2007**, *76* (4), 041135.
(59) Laskowski, R. A.; Swindells, M. B. LigPlot+: Multiple Ligand-Protein Interaction Diagrams for Drug Discovery. *J. Chem. Inf. Model.* **2011**, *51* (10), 2778−2786.

DOI: 10.1021/jacs.9b03703
J. Am. Chem. Soc. XXXX, XXX, XXX−XXX